applied sciences

MDPI

Article

A New Influence Mechanism of Clocking Effect in Subsonic Compressor

Han Niu, Jiang Chen * and Hang Xiang *

School of Energy and Power Engineering, Beihang University, Beijing 100191, China; niuhanbuaa@163.com
* Correspondence: chenjiang27@buaa.edu.cn (J.C.); xhyyyh@buaa.edu.cn (H.X.)

Abstract: This paper investigates the clocking effect in subsonic compressor element stages and the influence of design parameters on the flow mechanism. We focus on the relationship between the wake-induced separation loss and wake mixing loss and the unsteady mechanism in the wake flow process without considering the transition through several steady and unsteady numerical simulations aimed at a series of subsonic compressor element stages. The simulation results indicate that the performance difference at various indexing positions depends on the relationship between wake mixing loss and wake-induced separation loss for different compressor designs and operating conditions. Furthermore, the pressure transport caused by the negative jet of the Stator 0 wake in Rotor 1 creates a local acceleration region called SFAF, and a decrease in its absolute flow angle reduces the Stator 1 separation. Sufficient rim work of the rotor at highly loaded operating conditions is the basis for generating an effective SFAF. Furthermore, the fore-loading blade of Rotor 1 significantly reduces suction surface pressure drop, and a small angle between the stagger angles of Stator 0 and Rotor 1 increases the unsteady rotor load caused by the upstream wake to the total rotor load, both of which enhance SFAF.

Keywords: clocking effect; subsonic compressor; wake pressure transport; local acceleration region; unsteady design

check for updates

Citation: Niu, H.; Chen, J.; Xiang, H. A New Influence Mechanism of Clocking Effect in Subsonic Compressor. *Appl. Sci.* **2023**, *13*, 10094. https://doi.org/10.3390/app131810094

Academic Editor: Giovanni Bernardini

Received: 3 August 2023
Revised: 2 September 2023
Accepted: 4 September 2023
Published: 7 September 2023

Copyright: © 2023 by the authors. Licensee MDPI, Basel, Switzerland. This article is an open access article distributed under the terms and conditions of the Creative Commons Attribution (CC BY) license (https://creativecommons.org/licenses/by/4.0/).

1. Introduction

The ultimate goal of turbomachinery designers is to improve its performance, with the traditional design method still using the steady method for aerodynamic design. A deep understanding of the unsteady flow mechanism is the key to the unsteady aerodynamic design to improve the performance of turbomachinery further. Although researchers will also use unsteady numerical simulation or experiment to explore the unsteady flow phenomenon, due to the strong complexity of the flow caused by a variable radial load distribution of the single blade and load matching between different blade rows, it is challenging to develop universal and guiding design criteria for some unsteady flow.

The clocking effect is the most well-known method to improve turbomachinery performance by utilizing unsteady interaction. This effect aims to change the relative circumferential position of adjacent homonymous rows with the same blade number to influence the flow field and performance. Since Walker [1] first used the clocking effect to study noise generation in a compressor, many researchers have investigated how the clocking effect of a compressor and turbine is related to performance. It is generally believed that in a turbine, the best stage efficiency can be obtained when the wake of the upstream blade attacks the leading edge of the downstream homonymous blade (CLLE configuration). Accordingly, the worst efficiency occurs when the wake passes through the mid-position of the downstream blade passage (CLMP configuration) [2–4].

However, the influence mechanism of clocking effect in a compressor is relatively complex. Indeed, Smith and Key [5,6] experimentally studied the performance of the clocking effect at different loading conditions and observed that the loss difference was

small for low load and design load, while it was quite obvious in the corner region for high load. Simultaneously, they claimed that the clocking effect might be more effective when the corner region is poor, but the closer to the stall margin, the weaker the clocking effect on performance. The results demonstrate that CLLE is the best configuration for design load while CLMP is the best for high load, as proven by Key et al. [7,8]. They also found an interesting phenomenon that at the design load condition the rear stator is more sensitive to the change in incidence caused by the rotor wake in CLMP, and the fore stator wake will suppress this response in CLLE, ultimately leading to a narrow and shallow wake of the rear stator. Additionally, Smith and Key [9] confirmed that hub corner separation is the most important influencing factor for the clocking effect at high load conditions.

Städing et al. [10,11] experimentally studied the clocking effect in a low-speed compressor with cantilevered stators wherever the Mach number did not exceed 0.26. They found that efficiency is sinusoidal with the change in indexing position and also found significantly different results from those in high-speed compressors. They concluded that the optimal performance was gained for low and design loads when CLMP was set. However, CLLE configuration demonstrated performance advantages for high loads. Regardless of the operating condition, the static pressure rise in CLMP is always higher than in CLLE. Nevertheless, the authors did not conduct a detailed analysis of the stator's response to the wake impact for high load and only proposed an explanation that turbulence in the incoming wake can help suppress separation for high load due to its ability to cause a transition in advance.

Dorney et al. [12] investigated the clocking effect in a 1.5-stage high-speed compressor and demonstrated that it improves efficiency by 0.6–0.7 in CLLE, and wake contains an inherently steady component. Additionally, this effect causes an unsteady pressure response, significantly impacting loss. In [13], the authors studied the clocking effect in a two-dimensional numerical simulation of blade profiles. The results revealed that when the fore stator wake flows along the pressure side of the rear stator, the optimal combination of high efficiency and low force amplitude occurs, and once the wake moves towards the suction surface, the loss increases significantly. Further, [14] studied the influence of axial spacing on the clocking effect in a low-speed compressor and highlighted that the minimum efficiency occurred with two larger ones of three spacing when the CLLE configuration was set. Nevertheless, CLLE affords the maximum efficiency with the smallest spacing. The two-dimensional research performed by Huang et al. [15,16] demonstrated the performance advantage of CLLE, and they found that the clocking effect determines the degree of interaction between the stator and upstream stator wake. Moreover, they claimed that the difference in embedded rotor loss is relatively small. Meanwhile, Key et al. [17] also believe that the rotor wake is not affected by the clocking effect and that the change of stage efficiency directly results from a change in downstream stator loss, which mainly depends on the suction side boundary layer behavior.

Mileshin et al. [18] showed that the clocking effect becomes weaker as the tip clearance increases, and [19] demonstrated that the clocking effect becomes stronger as the Reynolds number decreases. Layachi and Bölcs [20] experimentally studied the influence of axial spacing variation on the clocking effect. In the tip region, the high fluid loss produced by the interaction between the IGV wake and rotor tip leakage flow becomes the most crucial loss influencing factor, and the stator loss is maximized in CLLE.

He et al. [21] used a numerical simulation method to investigate the clocking effect in subsonic and transonic compressors. CLLE is the configuration with the best performance, and in their opinion, it only comes down to the impact of the wake mixing loss. When the upstream wake passes through the position just above the suction surface where the shock wave has maximum intensity, due to the higher intensity of the shock wave, the interaction loss between the wake and the shock wave increases. Fruth [22] further demonstrated the impact of the mixing loss by suggesting that although the impact of the wake on the leading edge of the blade thickens the boundary layer, resulting in a wider and deeper wake different from that of [7,8], the total loss is minimal.

Jia and Vogeler [23] experimentally studied the effect of clocking on the unsteady embedded rotor load and pointed out that the time average pressure distribution on the rotor blade is difficult to notice, but the unsteady pressure fluctuations are significant. Hsu and Wo [24] studied the rotor clocking effect's influence on the stator's forced response. The method to reduce the stator response is to index the downstream rotor so that the moment when the contribution of upstream wake disturbance reaches the maximum is consistent with the moment when the minimum value of downstream potential disturbance occurs. Mailach et al. [25–27] investigated the clocking effect on the unsteady pressure fluctuations on the embedded rotor, and their experiments revealed that the efficiency change is less than the measurement uncertainty. Barankiewicz and Hathaway [28] also believe that the clocking effect has a small impact on compressor performance, probably due to the assembly tolerances of the test compressor.

As mentioned above, the two configurations are especially valued, although not all the optimal indexing positions are located at these two positions. In transonic compressors, the influence mechanism in transonic flow is relatively clear. In subsonic compressors, based on the above research, we find that the optimal clocking configuration for a high-speed compressor with shrouded stators for high load is CLMP because the wake impinging on the leading edge of the blade will result in increased corner separation. Moreover, the loss in the corner region is much greater than that at the other blade span. However, in other cases, multiple physical mechanisms interact, and the optimal configuration depends on which mechanism plays a dominant role. Hence, this paper conducts a series of steady and unsteady simulations evaluating the clocking effect of subsonic compressor element stages. Additionally, a new mechanism of improving performance by wake indexing is studied.

2. Research Objectives and Numerical Method

2.1. Research Objectives

The clocking effect in the three-dimensional environment can be divided into three categories: two-dimensional profile characteristics and the comprehensive effect of their radial superposition, the effect on corner flow, including leakage flow, and the change of three-dimensional flow caused by the phase differences in the indexing positions of different radial cross-section blade profiles. The existing research suggests that the clocking effect mechanism is not always consistent in subsonic compressors. Therefore, we focus on the clocking effect of a subsonic compressor element stage. Our research is mainly divided into two parts. First, we study the direct impact, mainly the relationship between the loss of wake-induced separation in CLLE and the wake mixing loss in CLMP without regard to transition. Then a new influence mechanism is discussed based on the indirect effect of an induced flow.

2.2. Mesh Generation

Throughout this research, we consider the same number of blades in each homonymous row, and AUTOGRID5 generated a structured mesh in NUMECA FINE/TURBO. The O4H-type mesh was used around the blade profile, and the pure H-type mesh was generated in both the inlet and outlet zones. Since the numerical simulation is two-dimensional, every case was set to a model with a height of 1 mm. Three points were set in the spanwise direction, and the height of the first layer from the solid surface was set to 1×10^{-6} m, ensuring that y+ is approximately 1.0.

2.3. Computational Fluid Dynamics Method

The numerical simulations were performed by the three-dimensional unsteady Reynolds-averaged Navier–Stokes (RANS) solver ANSYS CFX, which uses a finite volume method to compute the flow field. The convection term uses a second-order discrete scheme, and the time difference scheme uses a second-order backward Euler scheme. The shear stress transport (SST) turbulence model is chosen. Stagnation pressure, stagnation temperature, and flow angle are set for the inlet boundary, and the outlet boundary is set to

averaged static pressure. The mesh on the periodic boundary is matched, all blade surfaces are adiabatic and non-slip, and both hub and shroud are free slip wall. One percent rotor passing period is a physical time step including five iterations.

2.4. Validations of Computational Fluid Dynamics Method

To validate the numerical method, we choose the transonic compressor Stage 35, designed by NASA Glenn [29]. The height of the first layer from the solid surface is set to 5×10^{-7} m to ensure that y+ is approximately 1.0 and the total grid nodes are 6.07 million. The calculated results and the experimental data are compared in Figure 1. The results indicate that the flow margin is higher than the experimental value. Moreover, the numerical efficiency and the pressure ratio in most operating conditions are slightly higher, and the compliance of the pressure ratio near the design point pressure ratio is excellent. Overall, the CFD software and the adopted calculation method fulfill our research's numerical accuracy requirements.

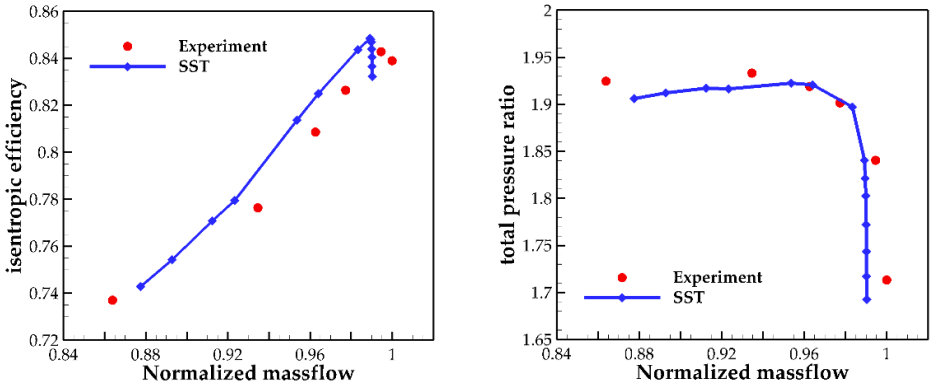


Figure 1. Performance comparison of the transonic compressor Stage 35. (**a**) Isentropic efficiency. (**b**) Total pressure ratio.

3. Direct Effect of Wake Indexing

When studying the stator clocking effect, the impact on the embedded rotor can be ignored in most instances. Further, when the upstream stator wake passes through the rotor, it is cut off and deflected. Thus, even if we can make the wake section hit the leading edge of the downstream stator, it cannot be guaranteed that the downstream stator's leading edge (LE) is always within the upstream stator wake. Therefore, we remove the embedded rotor to simplify studying the effect of streamwise wake indexing on the downstream stator and consider only the effect of the rotor wake on the downstream stator as an increase in incidence. It is worth noting that after the upstream stator wake passes through the rotor, the time-averaged flow angle in the wake differs from that in the bulk flow. Therefore, we ignore it and only consider the upstream stator wake as a flow with a velocity deficit relative to the bulk flow.

3.1. Geometric Parameters

The numerical simulations were performed with a baseline blade profile specially designed for this work using the controlled diffusion airfoil (CDA) generation program compiled by our research group. The corresponding profiles are illustrated in Figure 2, and the basic geometric parameters are reported in Table 1. In the simulation of loss characteristics, the inlet boundary is 0.7 times the chord length upstream of the LE, and the outlet boundary is 2 times the rotor chord length downstream of the trailing edge (TE). This setup aims to weaken the influence of numerical reflection. Moreover, the inlet and the axial section that is 0.4 times the chord length are chosen as the parameters' extraction location. The loss characteristics of the baseline blade profile are depicted in Figure 3, which

presents the total pressure loss as a function of incidence. A steady simulation of three Mach numbers was conducted. We studied the −6, 0, and 6 degrees of incidence at Ma 0.7 as operating conditions, with the three operating conditions called low load (LL), nominal load (NL), and high load (HL). The total pressure loss coefficient is defined below, and the time-averaged value is used in the unsteady results.

$$\overline{\omega} = \frac{\overline{p_{in}^*} - \overline{p_{out}^*}}{\overline{p_{in}^*} - \overline{p_{in}}} \tag{1}$$

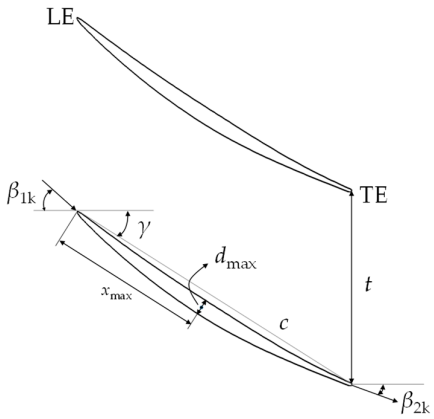


Figure 2. Schematic of the baseline blade profile.

Table 1. Geometric parameters of the blade profile.

Parameters	Symbol	Value
Chord/mm	c	40
Inlet blade angle/(°)	β_{1k}	42
Outlet blade angle/(°)	β_{2k}	0
Camber angle/(°)	$\Delta\beta_k$	42
Stagger angle/(°)	γ	21.25
Pitch/mm	t	22
Solidity	t/c	1.818
Maximum thickness/chord	d_{max}/c	0.048
Maximum thickness position/chord	x_{max}/c	0.52

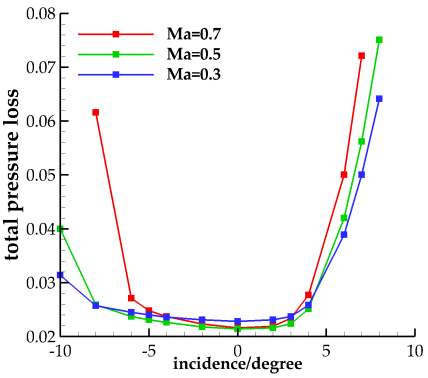


Figure 3. Loss characteristics of the baseline blade profile.

Grid independence is validated through four grid settings progressively refined in the flow and circumferential directions. The total grid number is 90 thousand, 180 thousand, 270 thousand, and 370 thousand, as depicted in Figure 4. By comparing the total pressure loss coefficient, the total grid number of 270 thousand is sufficient. Other examples in this paper also use this method for grid independence verification.

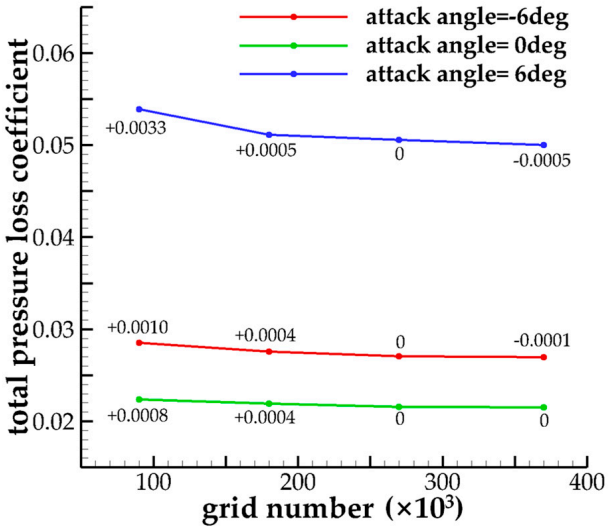


Figure 4. Validation of grid independence of the baseline blade profile.

3.2. Steady Analysis

Although the wake model [30] and wake generator [31] have been applied to study the unsteady interaction, the number of unsteady calculations to discriminate trends is unbearable. Thus, we use steady numerical simulation for trend determination. Note that the wake's velocity model is unsuitable for simulating compressible flow, as it can result in drastic changes in inlet parameters. If a wake generator generates a wake of different widths and depths, it becomes very complex for trend prediction. Therefore, we propose an alternative solution: to simulate the wake with the total pressure deficit as a quadratic function at the inlet. Although the velocity deficit it generates differs from the actual wake, this is sufficient for trend prediction during steady simulation.

Three wake widths were set in three operating conditions, with ratios of 0.1, 0.3, and 0.5 to pitch, respectively. For each wake width, we set three maximum total pressure deficit values, i.e., 10 kPa, 20 kPa, and 30 kPa, that generate velocity deficit of approximately 13%, 32%, and 62%, respectively, at the wake centerline (see Figure 5). In the calculations, we ensure that the Mach number of the bulk flow at the inlet is 0.7, and both CLLE and CLMP configurations can be generated by changing the position of the wake centerline.

Figure 6 illustrates the difference in total pressure loss between CLLE and CLMP. Overall, the loss of CLMP tends to be larger when the load is lower, while the loss of CLLE tends to be larger when the load is higher. Figure 7 depicts the pitch-wise distribution of the difference in total pressure loss between CLLE and CLMP at 0.4 times the chord length downstream of the blade. The naming method of the comparative cases and the expression method of upstream wake used next are the same as in Figure 7. In all comparative cases, the loss of CLLE is larger near the wake region, and the upstream wake passing through the passage will increase the loss in the area. Thus, the difference in total loss depends on the balance between these two types of loss.

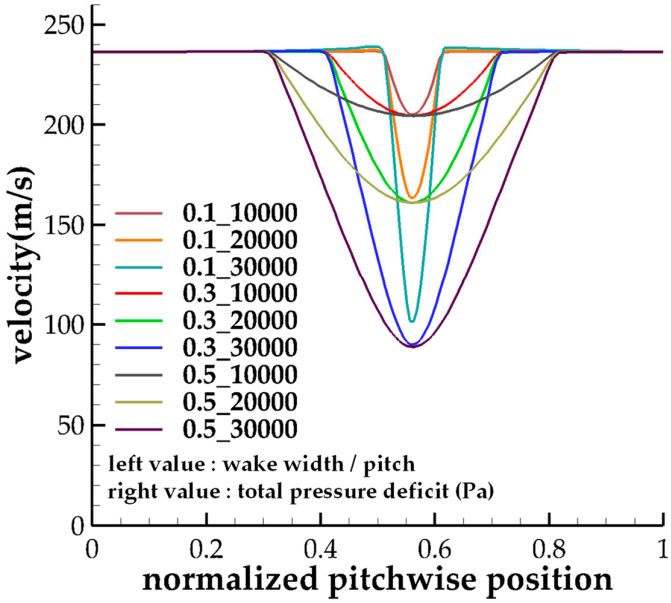
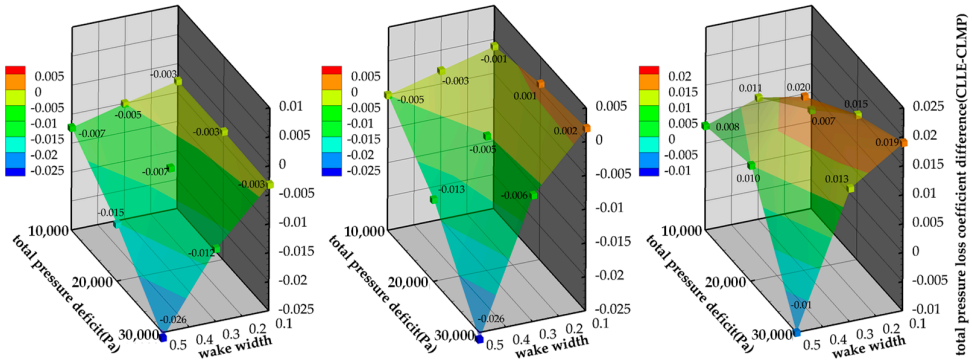


Figure 5. Wake velocity profile at the inlet in steady simulation.



(**a**) LL. (**b**) NL. (**c**) HL.

Figure 6. Difference in total pressure loss between CLLE and CLMP.

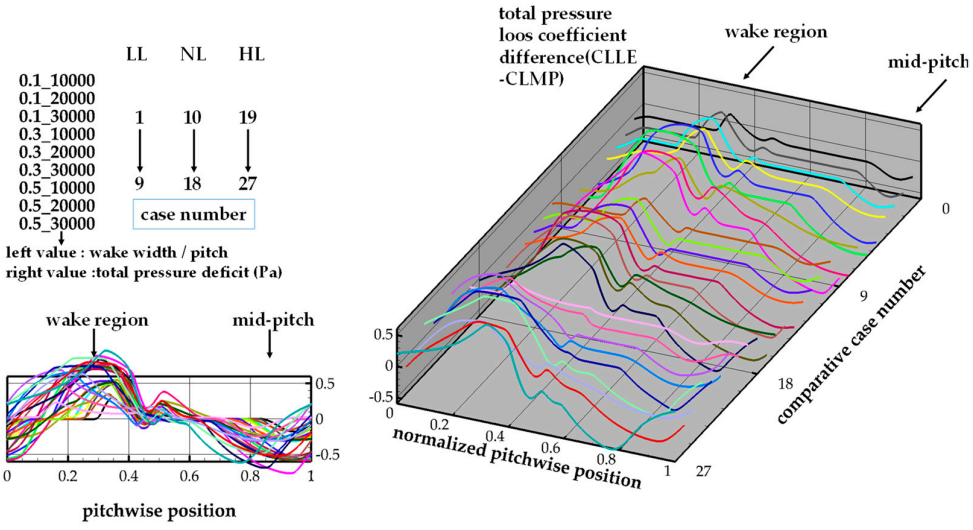


Figure 7. Difference in total pressure loss between CLLE and CLMP at 0.4 times chord downstream of the blade.

Figure 8 depicts the Mach number with 0 degrees of incidence, highlighting that the Mach number of the upstream wake is higher than 0.5. If the incoming flow is uniform, there is a small flow separation. However, as long as an upstream wake hits the LE of the blade, the separation will increase in size, and the larger the wake velocity deficit, the bigger the separation region. Hence, combined with Figure 9, we conclude that the upstream wake will reduce the velocity of the boundary layer, and the boundary layer cannot resist the reverse pressure gradient that is not significantly changed before the 0.7 axial chord. In this example, the bulk flow is the dominant flow of the whole flow field, and the upstream wake is a deceleration disturbance. Thus, we firmly believe that when the upstream wake width is greater than 0.5 times the pitch, the upstream wake is the dominant flow, and the bulk flow becomes an acceleration disturbance. Thus, when the bulk flow attacks the LE, it accelerates the boundary layer and reduces flow separation. Figure 10 compares the static pressure rise coefficient and reveals that the upstream wake attacking the LE always results in a lower diffusion capability.

$$C_p = \frac{p_{out} - p_{in}}{p_{in}^* - p_{in}} \tag{2}$$

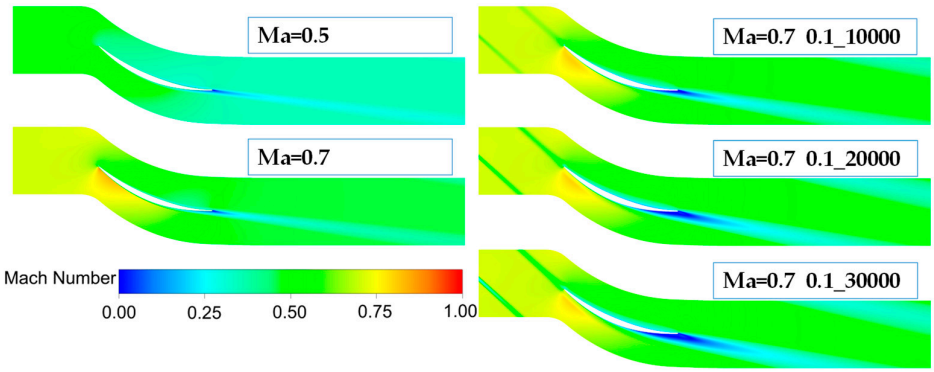


Figure 8. Mach number with 0 degrees of incidence.

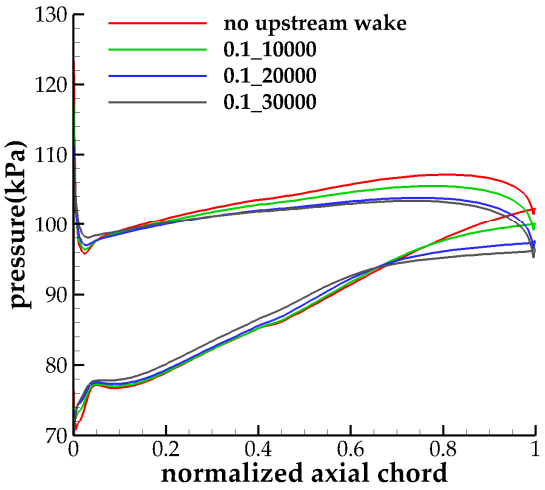


Figure 9. Pressure distribution of the chosen cases.

3.3. Unsteady Analysis

From steady analysis, we obtained the performance difference between CLLE and CLMP. However, the wake velocity profile assumption must be verified to determine the relative magnitude of the mixing loss. As mentioned earlier, the wake velocity model is not applicable, and the cylindrical wake generator typically used generates strong flow distortion due to flow stagnation (see Figure 11). Hence, we need a wake generator that

ensures the velocity and flow angle of the bulk flow are as uniform as possible to highlight the effect of the wake and generate a controllable wake. Therefore, we designed a new type of wake generator, as illustrated in Figure 12, which adds an extremely thin blade with a length of 12 mm in the direction of the incoming flow on a regular cylinder that slows down the fluid originally supposed to stagnate by adjusting the appropriate surface roughness. This phenomenon weakens the flow distortion caused by flow stagnation. At the same time, we also obtain different wake widths and depths by changing the radius of the cylinder and the surface roughness. Figure 12 reveals that the new wake generator can generate a uniform bulk flow.

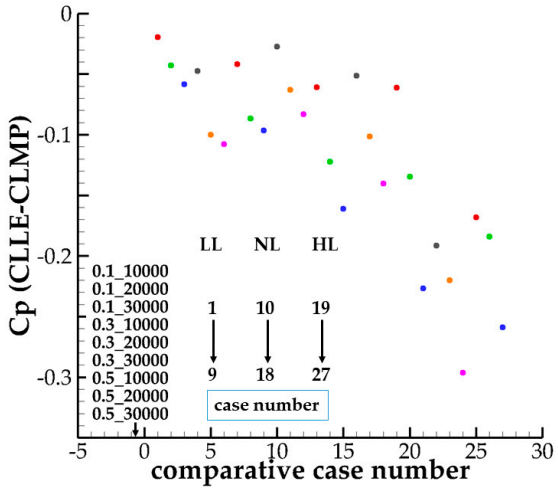


Figure 10. Difference in static pressure rise coefficient between CLLE and CLMP.

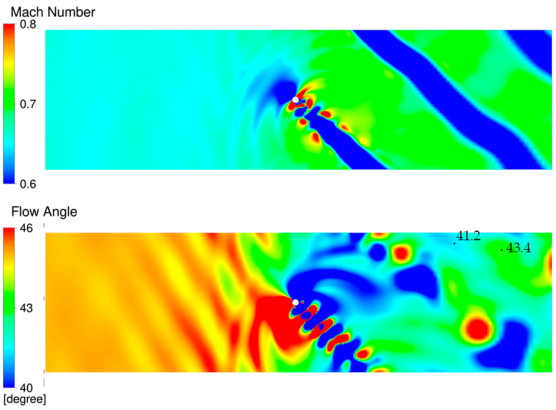


Figure 11. Cylindrical wake generator (diameter = 1 mm, pitch = 22 mm, Ma = 0.66, flow angle = 45 degree).

We connect the wake generator and baseline blade profile to form a tandem cascade under the settings listed in Table 2, and the Mach number of bulk flow at the outlet of the wake generator is 0.7. This case is named 0.4_50_LL_CLLE. The four items represent cylinder diameter, axial spacing, operating condition, and wake position. Figures 13–15 indicate that the difference in inlet parameters between CLLE and CLMP is negligible for each configuration and that the new wake generator can generate a uniform bulk flow to ensure the comparison effect. The performance parameters in Table 2 indicate that when the blade load is lower, the flow separation loss caused by the wake in CLLE is easily lower than the wake mixing loss in CLMP. Combined with steady analysis and from the perspective of flow separation loss, CLLE always has a negative effect, but the total loss of CLLE can be lower than that of CLMP. As the flow angle increases, it is difficult to make the total loss of CLLE lower than that of CLMP because the flow separation on the suction surface intensifies, and the loss becomes larger.

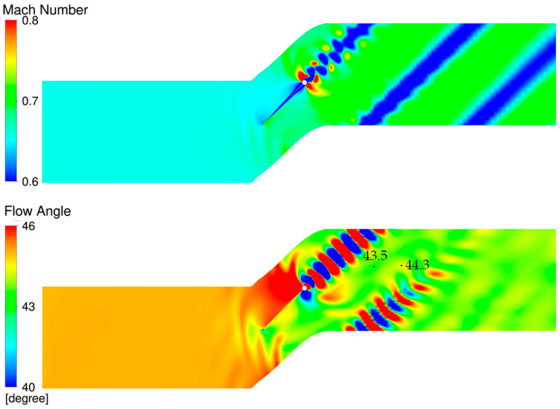


Figure 12. New wake generator (diameter = 1 mm, pitch = 22 mm, Ma = 0.66, flow angle = 45 degrees, sand grain roughness height = 100 micron).

Table 2. Unsteady case settings and performance comparison.

Cylinder Diameter/mm	Axial Spacing/mm	Operating Condition	Sand Grain Roughness Height/Micron	$\overline{\omega}$ CLLE	$\overline{\omega}$ CLMP
0.4	50	LL	20	0.027	**0.030**
0.4	50	NL	20	0.023	**0.024**
0.4	50	HL	20	**0.047**	0.044
1.5	50	LL	300	0.048	**0.057**
1.5	50	NL	300	0.046	**0.054**
1.5	50	HL	300	**0.069**	0.068
1.5	100	LL	300	0.027	**0.031**
1.5	100	NL	300	0.025	**0.030**
1.5	100	HL	300	**0.068**	0.060

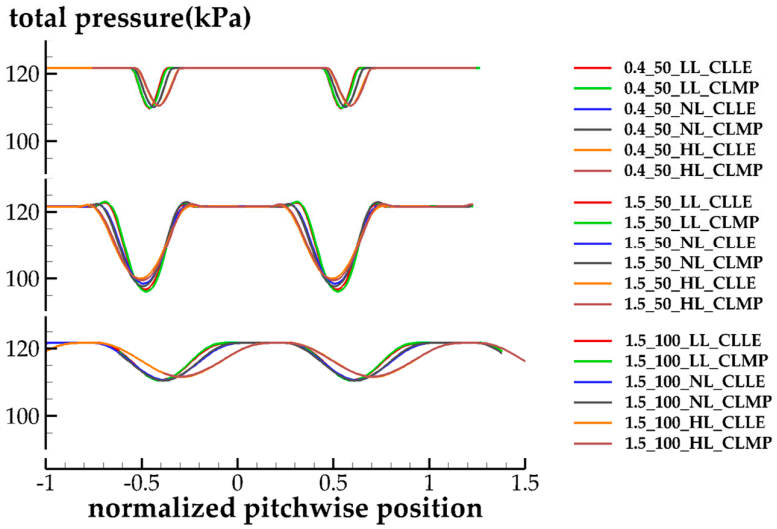


Figure 13. Total pressure comparison (0.7 chord length before the LE of the baseline blade).

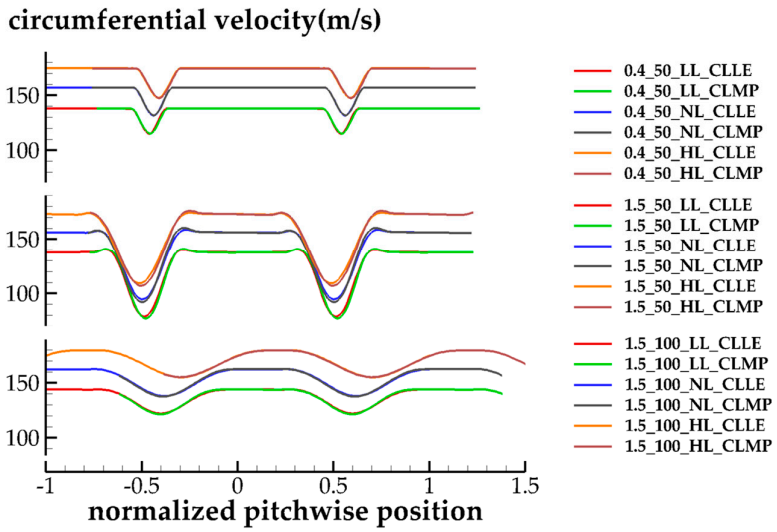


Figure 14. Circumferential velocity comparison (0.7 chord length before the LE of the baseline blade).

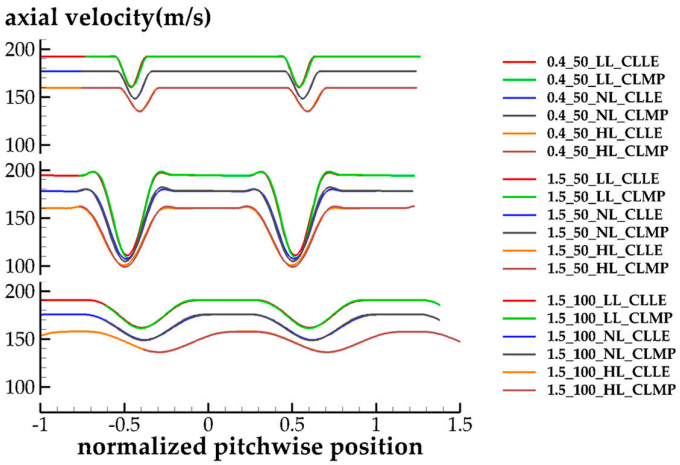


Figure 15. Axial velocity comparison (0.7 chord length before the LE of the baseline blade).

For the clocking effect, if the transition induced by the upstream wake is not considered at the high load condition, the CLLE will generally make the flow separation on the suction surface greater, which is consistent with the conclusion obtained in this section.

4. Influence Mechanism of Induced Flow

In a subsonic compressor, the loss characteristic of the cascade indicates that at high incidence, the loss varies greatly with the incidence, exceeding the sensitivity to Mach number. Thus, if the upstream flow contains a mass of fluid with a low flow angle, the configuration can be the indexing position of the lowest loss when the fluid mass hits the LE of the downstream blade at the operating condition of high incidence.

4.1. Analysis of the Baseline Stage

This study considers a 1.5-stage subsonic compressor element stage where the baseline stage is modified from the stator of the fifth and sixth stage of an 8-stage low-pressure compressor. The three rows of blades are Stator 0 (S0), Rotor 1 (R1), and Stator 1 (S1), all of which use uniform loading. For R1, we will not make any changes to ensure the original blade profile and solidity. For S0, it only provides pre-whirl and wakes for the rotor. Its blade number is changed to be the same as R1 to reduce the computational burden, and the reduced solidity has an additional advantage in adjusting the wake size by slightly changing the incidence. It should be noted that this study relies on the flow phenomenon discovered in

previous research on rotor–stator interaction with S0 and R1. Figure 16 and Table 3 present all blade profiles and geometric parameters.

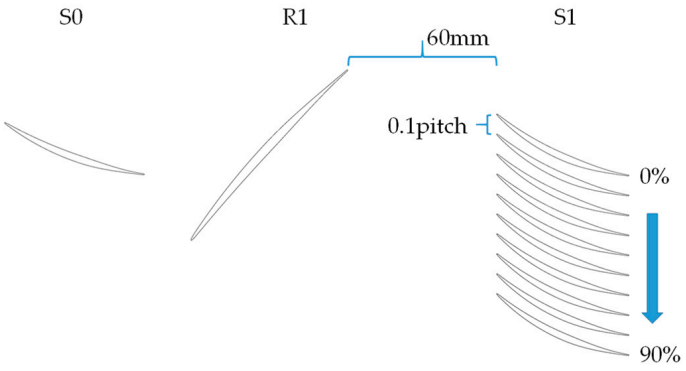


Figure 16. Profile and design parameters of the baseline stage.

Table 3. Geometric parameters of the baseline stage.

Parameters	S0	R1	S1
Chord/mm	61.4	95.2	62.8
Inlet blade angle/(°)	33.4	53.8	42.8
Outlet blade angle/(°)	7.8	41.3	17.6
Stagger angle/(°)	20.3	47.4	30.0
Pitch/mm	82.1	82.1	82.1
Solidity	0.75	1.16	0.76
Rotational speed/(m/s)	/	246.3	/
Blade passing frequency	/	3000	/

For the stator–rotor configuration comprising S0 and R1, we set three deep wakes by slightly adjusting the incidence of S0, whose value is just 1 degree for three R1 operating conditions: low, nominal, and high. Figure 17 illustrates the absolute flow angle distribution of the results, with dashed lines representing the upstream wake. In every case, the local fluid mass of a small flow angle appears immediately following the upstream wake centerline. We will refer to it as SFAF for the remainder of this work. In LL, the SFAF is located near the pitch's center line and close to the pressure surface. As the upstream wake depth increases, this position is closer to the pressure surface, and its flow angle decreases more than the bulk flow. In NL, the traverse range of the SFAF increases, but the difference in flow angle with the bulk flow does not significantly increase. Meanwhile, the flow angle in the upstream wake section gradually increases. In HL, as the upstream wake depth increases, the position of the SFAF does not change much, and the flow angle decreases sharply. However, the flow angle increase in the upstream wake section, which is close to the SFAF, is also significant. Overall, the upstream wake at its location is twisted, and the greater the decrease in the SFAF inflow angle, the more severe the twist of the upstream wake. According to Figure 18, an increase in relative velocity leads to a decrease in the absolute flow angle of the SFAF.

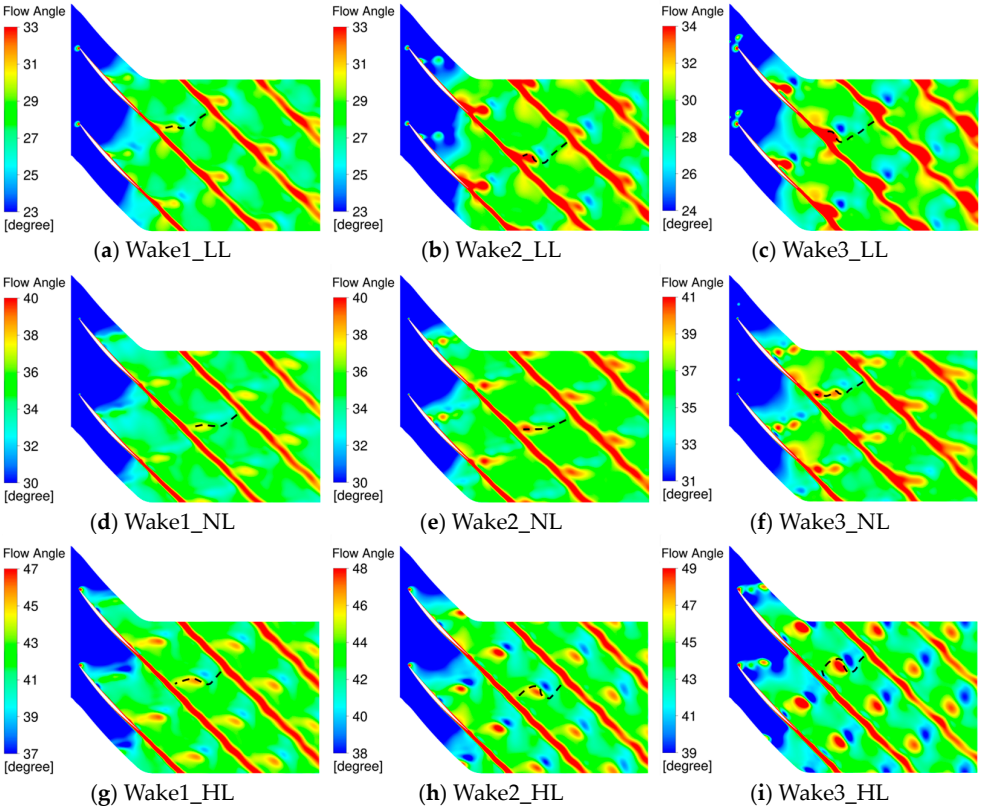


Figure 17. Absolute flow angle of R1.

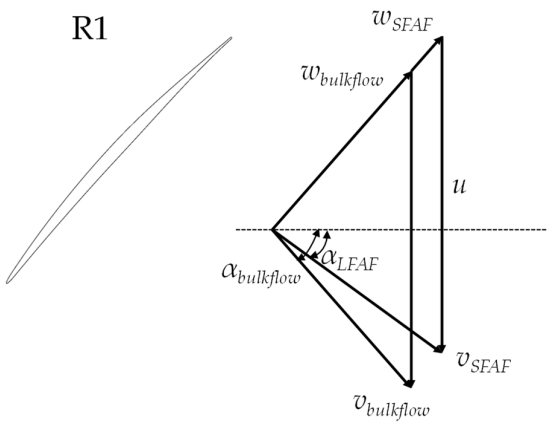


Figure 18. Principle of increasing the flow angle of the fluid mass.

To explore the mechanism producing SFAF, we use monitoring points on the stream surface at mid-span to obtain time-resolved data, as illustrated in Figure 19. The method to generate the monitor points is based on a parameterized blade profile, as proposed in our previous study [32]. The monitor points are set in the rotor, and the axial spacing from the rotor–stator spacing to the LE. Two hundred points are in the circumferential direction with uniform distribution from the suction side of one blade to the pressure side of the adjacent blade, and the monitor points that cross the mesh boundary are transformed to the inside of the computational domain. In the axial direction, there are six uniform monitor points from the LE to the TE, and two uniform points are set before the LE, the first of which is 0.4 mm after the interface.

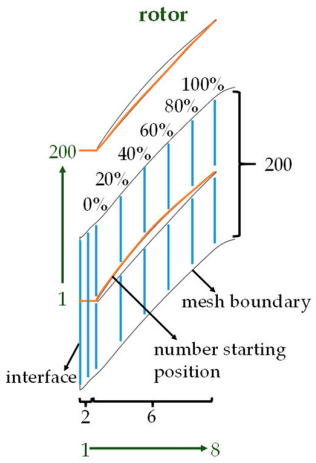


Figure 19. Monitoring points setup.

The Wake3_LL, Wake3_NL, Wake3_HL, and Wake2_HL cases are used to analyze and collect the monitoring data of the two-blade passing period (BPF). Figure 20a illustrates the schematic pressure transport. Figures 21–25 present the time-varying pressure and relative velocity at the axial monitoring stations. The black solid line represents the approximate contour of the wake obtained from the data of the time-varying entropy, representing different moments when the same wake passes through the same axial position. The first subgraph of Figure 21 illustrates a low-pressure region downstream of the wake, which does not completely coincide with the wake but leans towards the downstream. This indicates that during the flow process of the wake in the rotor flow field, the low-pressure fluid generated by the accelerated flow near the suction surface is transported towards a certain angle downstream of the wake. From the second subgraph of Figure 21, the pressure in the wake transport direction further decreases, and the transport path almost starts from the suction surface. At 0% axial chord, the low-pressure region has been locally strengthened at the 50% position, indicating that any position in the wake segment can produce a local low-pressure region by transporting fluid at the local location it flows through. This occurs if the local pressure gradient in the wake transport direction is positive. However, the flow transport starting from the suction surface is also the backbone. At 20% axial chord, the pressure transport phenomenon still exists but gradually becomes indistinguishable. Combined with Figure 22, due to the low-pressure region mentioned earlier, the velocity of the fluid upstream of the wake section increases, causing a pressure drop at the corresponding position. The fluid mass with the largest increase in velocity distorts the wake section. Meanwhile, the wake section always obstructs the accelerating fluid mass. At 100% axial chord, the flow acceleration upstream of the wake section has a range exceeding 65% pitch near the suction surface. Combined with Figures 17c and 18, the position with the highest acceleration has the lowest absolute airflow angle.

Figures 23 and 24 present the time-varying pressure and velocity. Due to the increase in load, the rotor flow angle increases from small to large, and the loading position gradually moves upstream. Thus, the location range of the low-pressure region generated by the wake transport moves ahead gradually, and especially in Wake3_HL, the low-pressure region is generated completely before the LE. Meanwhile, SFAF has a stronger acceleration ability and can gradually resist the obstruction of the wake and cross the wake gradually as the load increases at 9.6 mm before the LE. At the same axial position, the low-pressure region can reach 90%, 70%, and 30% pitch in the pitch-wise direction in Wake3_LL, Wake3_NL, and Wake3_HL, respectively, because as the load increases and the flow rate decreases, the transport speed of the wake in the rotor flow field also decreases. Therefore, the lower the load, the larger the range of SFAF upstream of the wake in the pitch-wise direction. Due to the angle between the direction of pressure transport and the wake, the closer the pressure surface, the greater the distance between the low-pressure region and the wake. The actual

effect of inducing the acceleration of SFAF is different, resulting in the maximum velocity increase in SFAF being related to the local pressure gradient. It is worth noting that we only consider the magnitude of the velocity increase and do not analyze the direction of the velocity increase in detail. The existing results indicate that the velocity increase in SFAF can decrease its absolute flow angle.

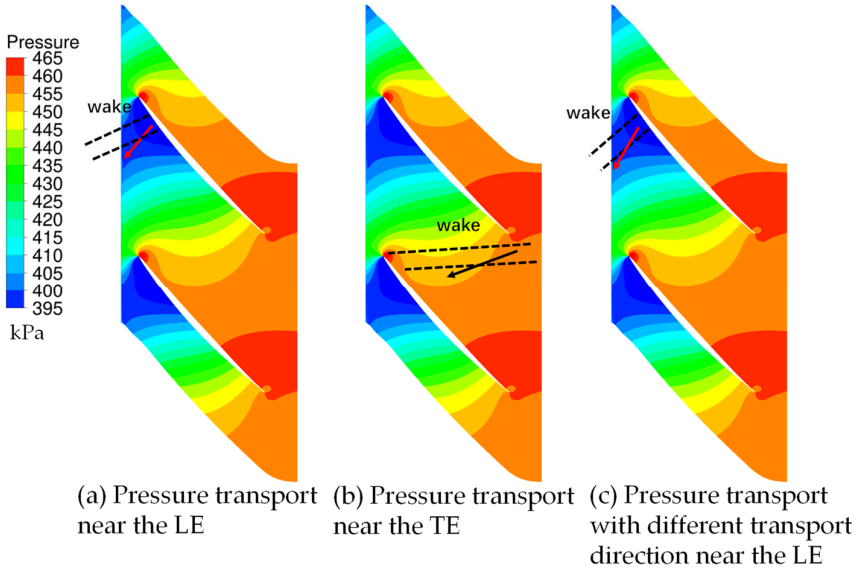


Figure 20. Schematic diagram of wake transport direction.

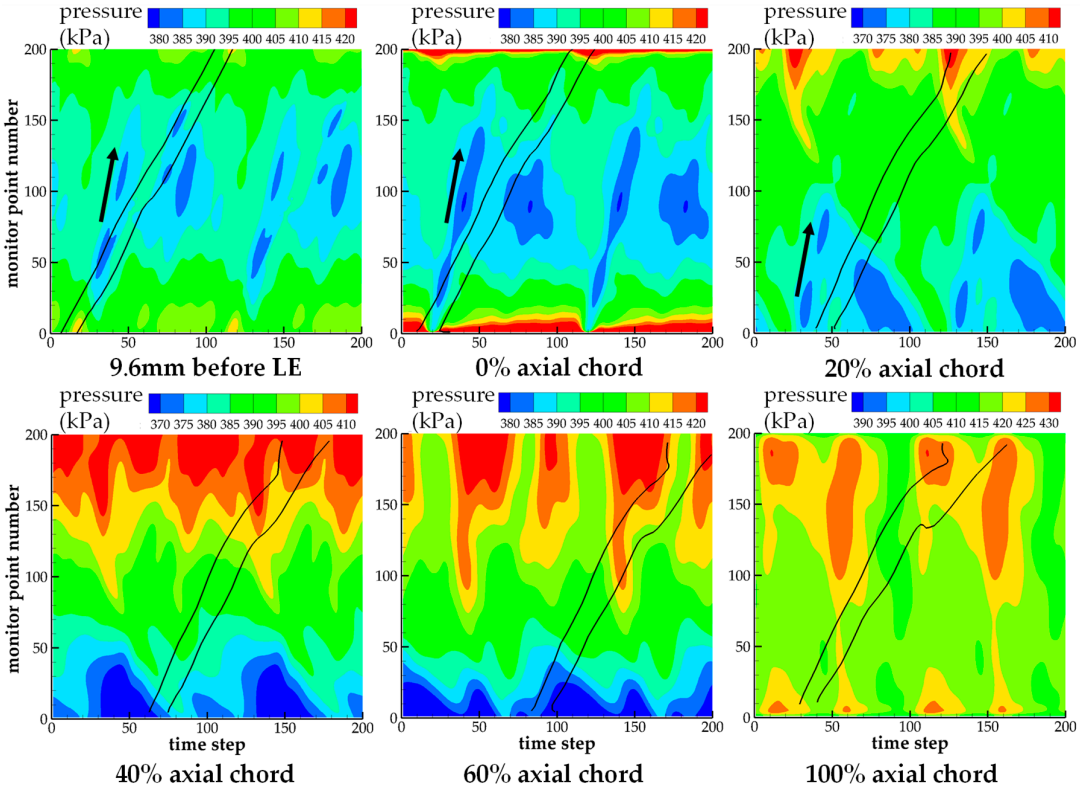


Figure 21. Time-varying pressure of Wake3_LL.

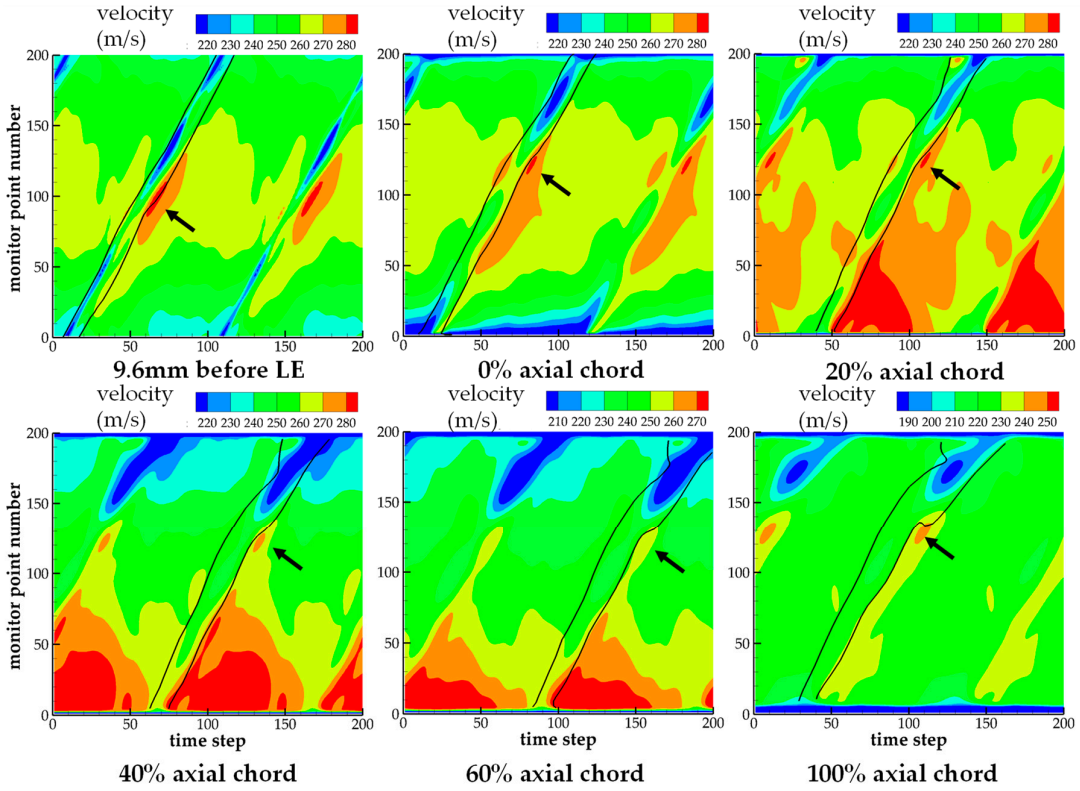


Figure 22. Time-varying velocity of Wake3_LL.

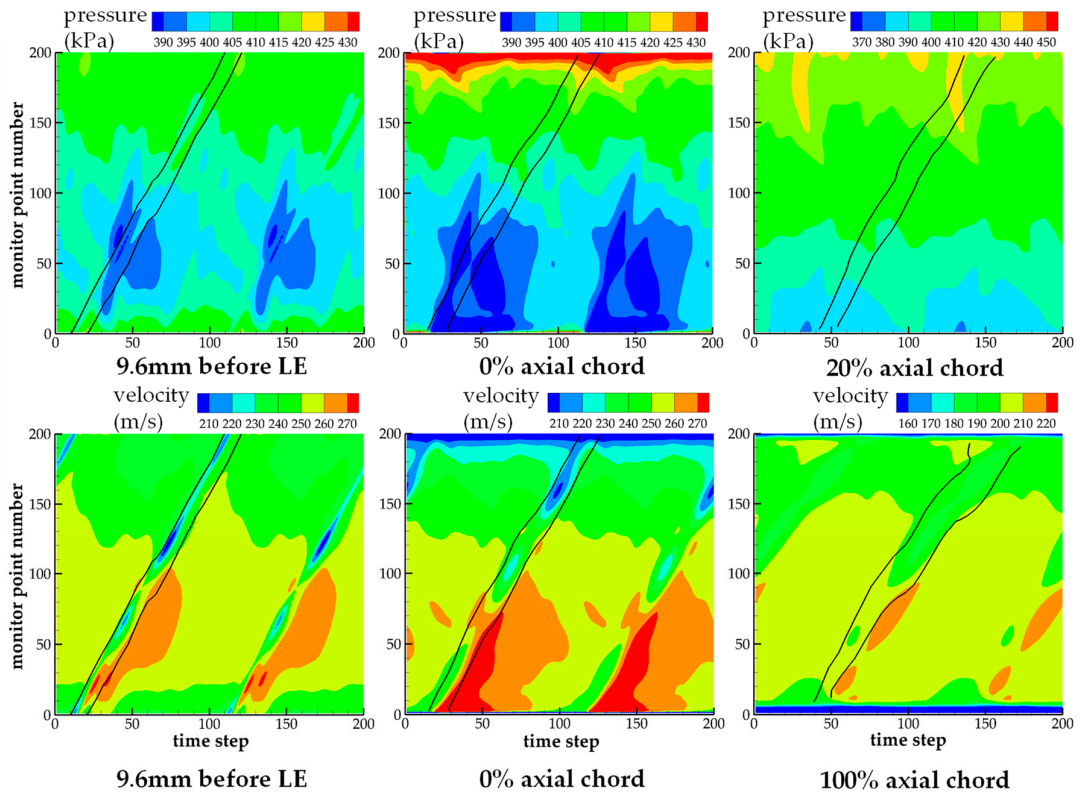


Figure 23. Time-varying pressure and velocity of Wake3_NL.

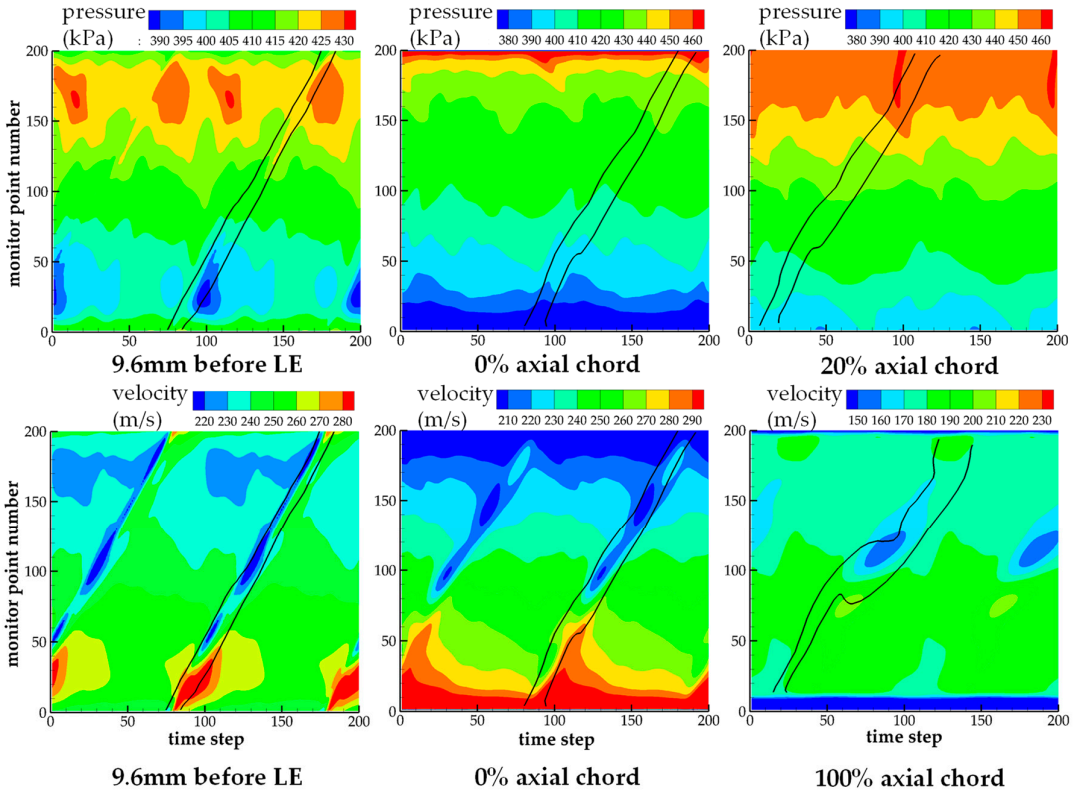


Figure 24. Time-varying pressure and velocity of Wake3_HL.

Figure 25 illustrates the time-varying pressure and velocity of Wake2_HL. Combined with Figure 24, it can be concluded that due to a shallower wake generated by S0 in Wake2_HL, the decrease in transport velocity of the wake decreases the circumferential range of the low-pressure region. Additionally, due to the positive angle of attack of the S0 wake relative to R1, the S0 wake in Wake2_HL results in relatively high pressure on the suction surface at the LE of R1, leading to relatively high pressure in the low-pressure region generated by the wake transport. Therefore, the velocity of SFAF is also relatively small. In summary, sufficient wake depth and a strong pressure gradient are necessary for forming a local low-pressure region.

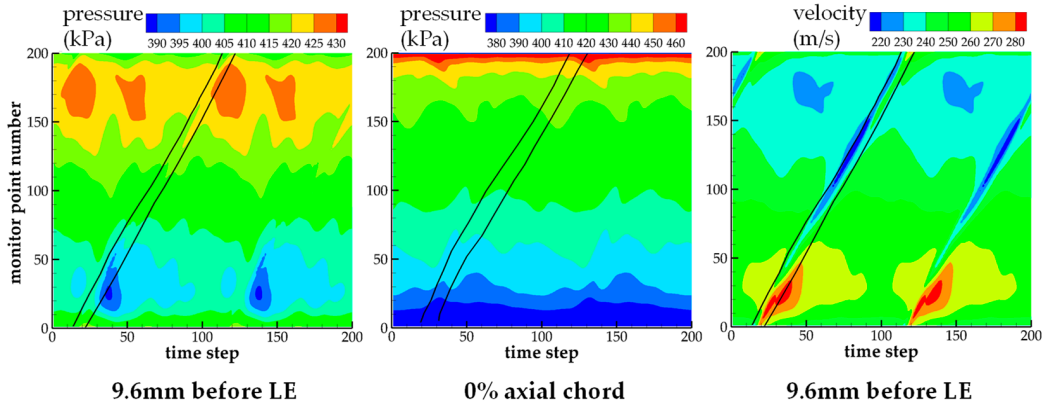


Figure 25. Time-varying pressure and velocity of Wake2_HL.

In a 1.5-stage compressor, if the SFAF impacts the LE of S1 at a large incidence, the small flow angle of the SFAF can reduce S1 separation, making this configuration the optimal indexing position. However, if we want to prove the effectiveness of SFAF in reducing losses, an S1 must be matched after R1. Based on existing compressor design experience,

the rotor–stator structure generally does not occur when the stator is simultaneously at a large positive incidence, and the rotor is at a large negative incidence. Although in the extensive calculations conducted in the early stage of this study, some similar SFAFs closely follow S0 wake with a relatively large circumferential range like that in Wake3_LL.

Therefore, we conduct a clocking effect study on the 1.5-stage, as depicted in Figure 16, where the axial spacing between R1 and S1 is set to 60 mm to weaken their potential interference and provide an observation area. Ten indexing positions with a circumferential spacing of 0.1 pitch are used for the calculations, and the flow rate of all cases is consistent with that of Wake3_HL. Figure 26 presents the results of the cases, and the time-averaged efficiency is defined as Function (3). The results infer there is not much difference in the time-averaged efficiency of S0-R1, and the maximum difference is only 0.18%, which can be ignored. The stage efficiency of the indexing position that SFAF impacts the LE of S1 is not the maximum but the local minimum. Note that we do not conduct extensive visual analysis on this, as the size and flow angle reduction of SFAF is insufficient.

$$\overline{\eta} = \frac{\left(\overline{p^*_{out}}/\overline{p^*_{in}}\right)^{\left(\frac{k-1}{k}\right)} - 1}{\overline{T^*_{out}}/\overline{T^*_{in}} - 1} \tag{3}$$

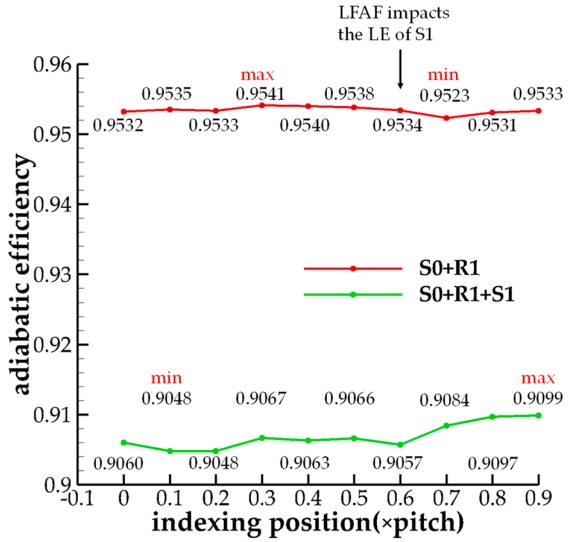


Figure 26. Performance of the baseline stage at the indexing positions.

4.2. Modification of the Baseline Stage

Next, strengthening the SFAF is required, but always matching S1 to verify the effectiveness of SFAF during the improvement process increases the computational burden. Therefore, we remove S1 and ignore the impact of S1 on R1. Additionally, we do not detail the evolution process of the velocity increment and direction caused by the low-pressure region. We only determine whether the range and absolute flow angle reduction behind the TE of R1 are sufficient based on experience. The discriminative experience is that SFAF always exhibits a relatively concentrated state during development. Meanwhile, it weakens more significantly with the twisted high absolute flow angle wake cluster called LFAF adjacent to SFAF during the flow process (see Figure 17i). Thus, we set up four modification plans to explore the strengthening effect of SFAF from a design perspective, all based on the baseline stage. During the modification process, we only considered the performance of SFAF at the operating condition when R1 is at large incidence.

4.2.1. Modification Plan 1: Wake Reduced Frequency

Equation (4) defines the wake-reduced frequency, representing the relative distance between adjacent wakes. Thus, the blade number of S0 is increased by 1.5 times and

2 times to control the reduced frequency of the wake. Two sufficient wakes are set for each configuration while ensuring the steady load of R1 is approximate to that of Wake3_HL.

$$F_r = \frac{u/t}{w_{out}/c} \tag{4}$$

The induced acceleration of the low-pressure region causes the formation of SFAF. If the reduced frequency of the wake is relatively high, the low-pressure regions generated by the adjacent two wakes are closer, weakening the acceleration ability of SFAF or connecting it into a whole. Note that its effect cannot be highlighted, as depicted in Figure 27.

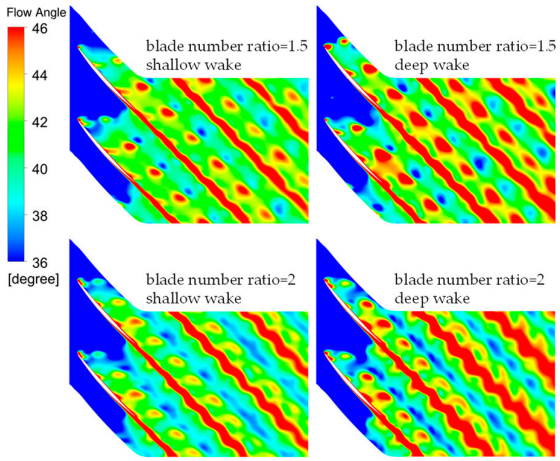


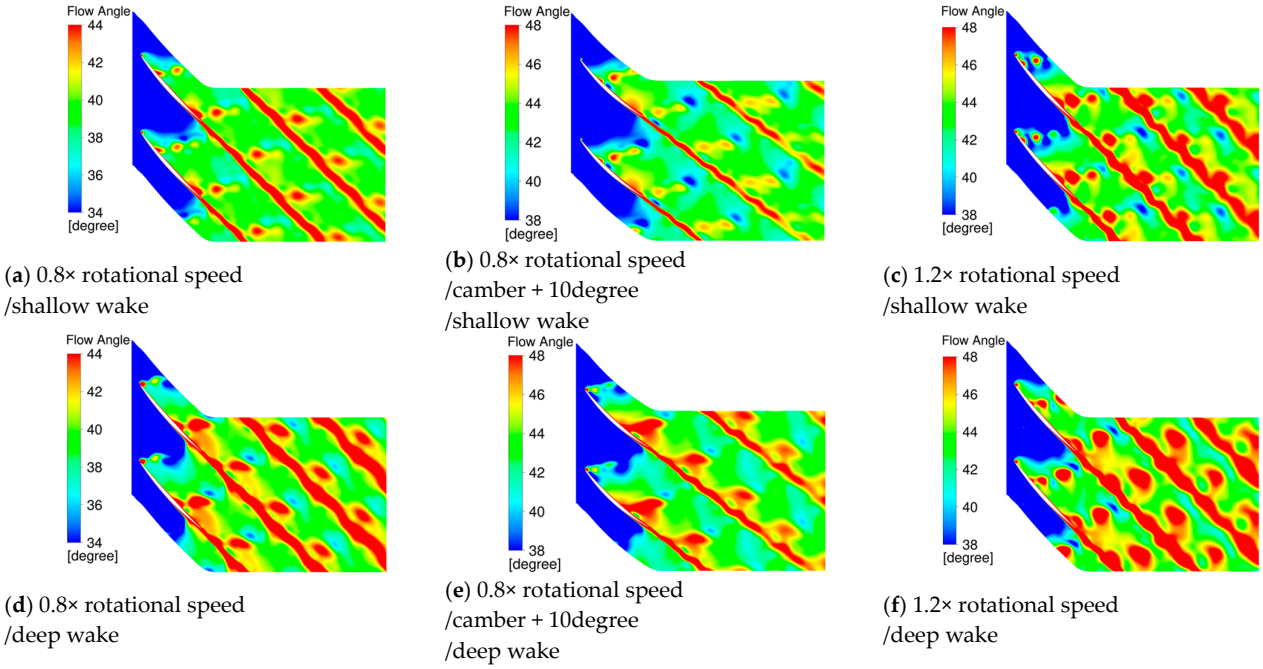
Figure 27. Absolute flow angle of modification plan 1.

4.2.2. Modification Plan 2: Rotor Load

The change in rotor power capability is achieved by modifying the rotational speed or camber angle. The rotational speed of R1 is changed to 0.8 times and 1.2 times the original value. For the former, there are two settings for the R1 camber angle, one remains unchanged, and the other increases the camber angle by 10 degrees by adjusting the outlet blade angle. For the latter, the R1 camber angle remains unchanged. Two sufficient wakes are also set for each configuration. Figure 28 depicts the absolute flow angle and the shallow wake, making SFAF the most significant. Thus, the deep wake is selected because it intensely weakens SFAF.

By comparing Figures 17i and 28a,c the effectiveness of SFAF in descending order is 1.0×, 1.2× and 0.8×. Hence, if the load is too low, the pressure drop near the LE's suction surface is insufficient, and the pressure transport effect is not obvious. If the total load increases by increasing the tangential velocity, according to Figure 18, even if the pressure transport effect is stronger, the acceleration of SFAF is more obvious. However, due to the large tangential velocity, the trend of the absolute flow angle reduction of SFAF is not easy to determine. By comparing Figure 28a,b, it can be inferred that if the total load is increased by increasing the camber angle, the pressure drop at the suction surface near the LE is greater, and the pressure transport effect is more obvious.

This study modified the tangential velocity and inlet and outlet blade angle to perform many cases, including the ones in this subsection. The trials verified that the level of total load affects the generation of SFAF by controlling the pressure drop at the front end of the suction, but it is not the only influencing factor. The relationship between the low-pressure region caused by wake transport and the velocity increase in SFAF is relatively complex in the flow field. However, the rotor tangential velocity and camber angle combination that can generate the best SFAF should be obtained through unsteady optimization.



(**a**) 0.8× rotational speed /shallow wake

(**b**) 0.8× rotational speed /camber + 10degree /shallow wake

(**c**) 1.2× rotational speed /shallow wake

(**d**) 0.8× rotational speed /deep wake

(**e**) 0.8× rotational speed /camber + 10degree /deep wake

(**f**) 1.2× rotational speed /deep wake

Figure 28. Absolute flow angle of modification plan 2.

By comparing Figure 28b,e, as well as Figure 28c,f, it reveals that when the incoming wake is too strong, not only is SFAF weakened, but LFAF is also strengthened. Considering the cases of 1.2× rotational speed as an example, Figures 29 and 30 show the time-varying pressure and velocity. Combined with Figure 20b, it can be concluded that when the incoming wake is deep enough, it can maintain a strong transport effect after flowing and decaying in the cascade passage. Thus, it will transport high-pressure fluid to a low-pressure location at the blade passage's rear end, resulting in nearby LFAF further deceleration. In summary, although the depth of the S0 wake increases, low-pressure fluid transport at the front end makes SFAF more pronounced. However, the high-pressure fluid transport at the rear end causes an increase in the absolute flow angle of LFAF, increasing the side effect of S0 wake on S1. Blindly strengthening the incoming wake is not an effective way to strengthen SFAF.

It should be noted that the separation degree of R1 should not be too high. Otherwise, the negative jet effect of the R1 wake will weaken the aggregation of SFAF.

4.2.3. Modification Plan 3: Rotor Loading Form

The previous section indicates that the global load level of the blade is not the decisive factor for generating SFAF. Based on previous analysis of the baseline stage, it can be concluded that the pressure reduction caused by flow acceleration of the blade suction surface near the LE is sufficient to generate a low-pressure region by wake transport. Moreover, at the high load condition, i.e., the fore-loading condition, the strengthening level of SFAF is higher. Therefore, it can be inferred that the more forward the loading position, the greater the pressure reduction of the suction surface near the LE. Thus, the uniform loading R1 was modified to the fore-loading profile, and the camber angle was increased by 5 degrees, as shown in Figure 31. In this way, at the condition with a similar inflow, the fore-loading blade can generate greater pressure reduction on the suction surface near the LE. An appropriate incidence was set for S0 to ensure a sufficiently deep wake was generated. The result of the high load condition with other settings unchanged is depicted in Figure 32, demonstrating a good SFAF reinforcement effect.

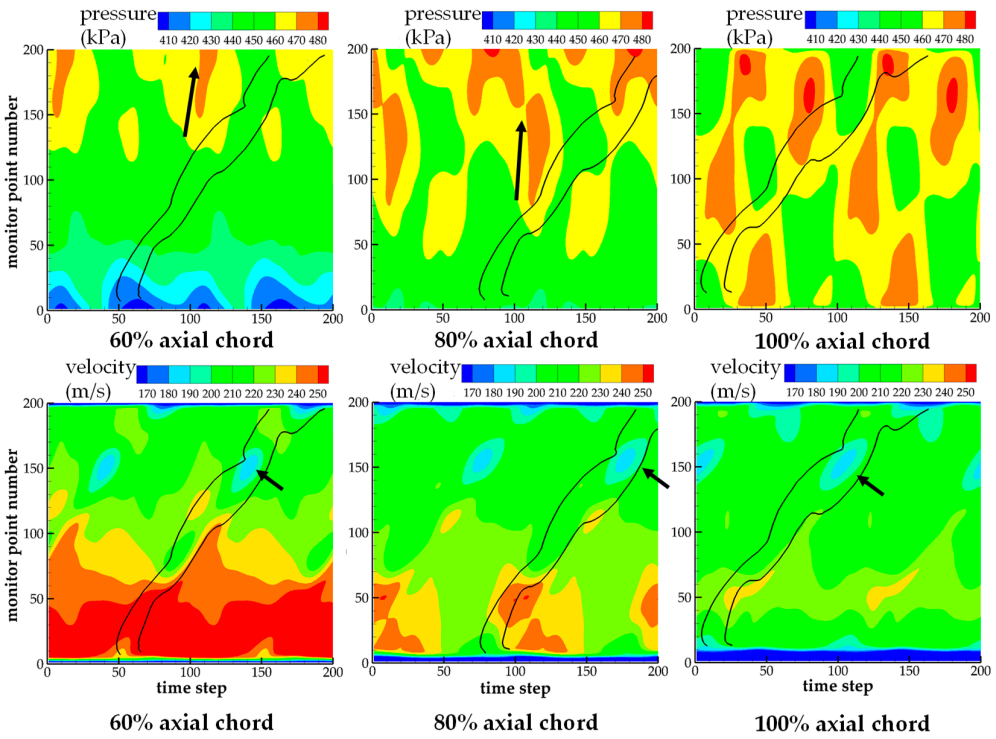


Figure 29. Time-varying pressure and velocity of the case of 1.2× rotational speed with an incoming shallow wake.

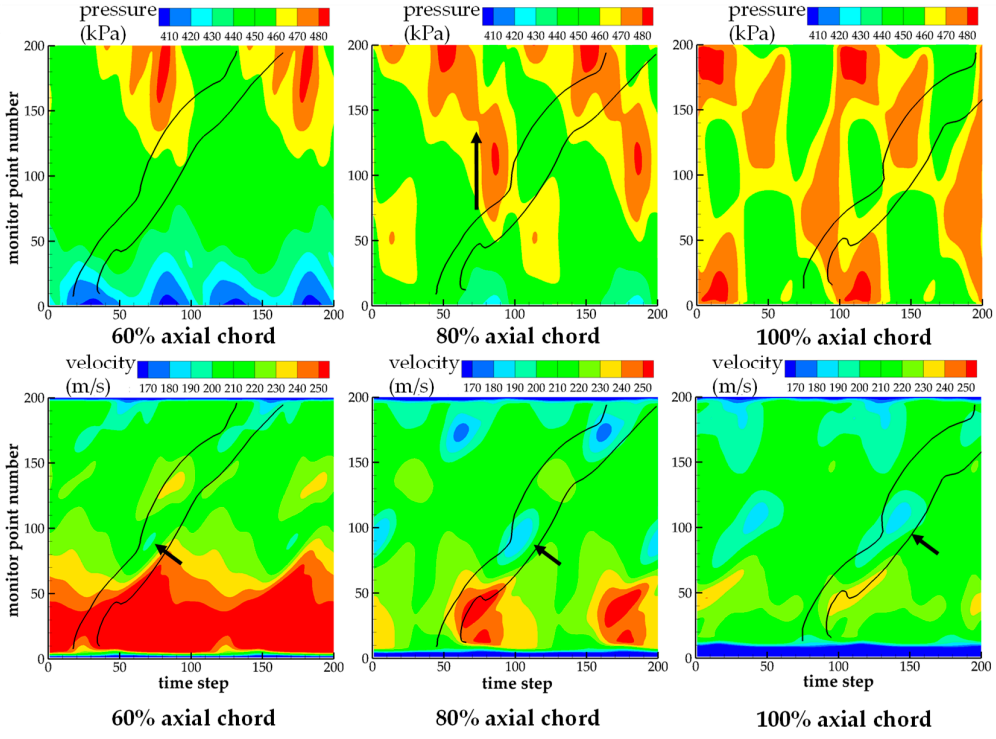


Figure 30. Time-varying pressure and velocity of the case of 1.2× rotational speed with an incoming deep wake.

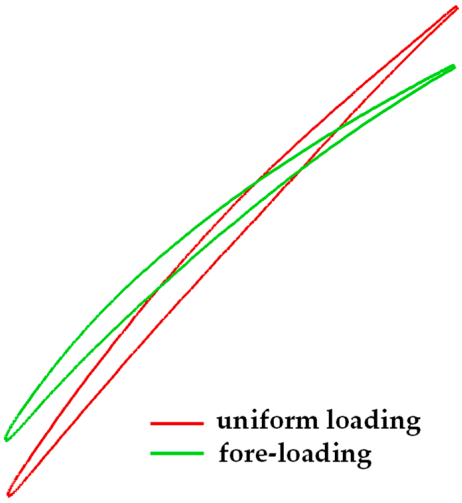


Figure 31. Comparison between uniform loading and fore-loading blade profiles.

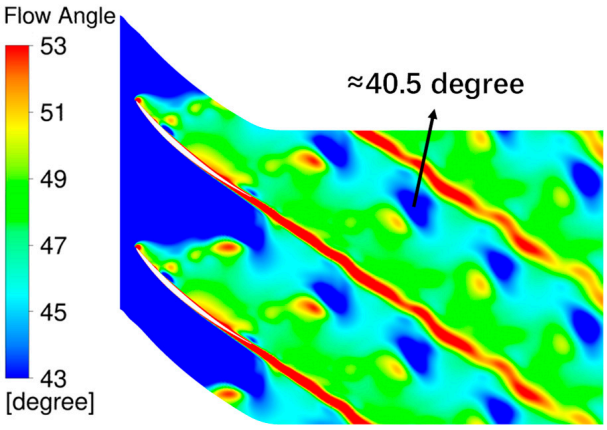


Figure 32. Absolute flow angle of modification plan 3.

Thus, an S1 was matched after R1, ensuring S1 had significant separation at the operating condition. It should be noted that SFAF aims to reduce the S1 separation loss. If the degree of separation and the proportion of separation loss is inadequate, the indexing position when SFAF impacts the LE of S1 is not optimal. All cases were calculated to the same flow rate, and Figure 33 reveals the performance results. At the indexing positions of 70%, 80%, 90%, and 0% pitch, the LE of S1 will all come into contact with the S0 wake, and at the first three positions, SFAF impacts the LE of S1 with varying degrees. Figure 34 indicates that SFAF weakens the positive incidence response of S1 at high load conditions, reducing separation and achieving the best efficiency at the indexing position of 80% pitch. According to the third part of this article, the impact of the incoming wake on the LE of the blade always leads to an increase in separation, and the transition is not considered in this study, thus highlighting the effect of SFAF. This result also confirms that due to the continuous attenuation during the wake flow process, the forward load reduces the pressure of the suction surface even more, resulting in a lower pressure of the local low-pressure region induced by the S0 wake at the moment of maximum transport intensity near the leading edge.

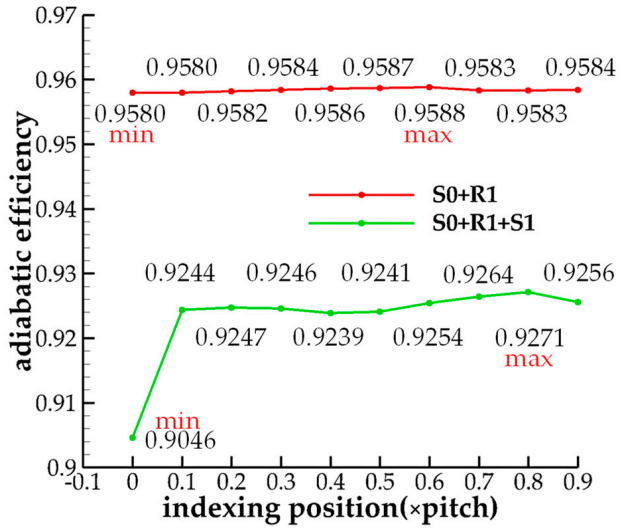


Figure 33. Performance of modification plan 3 with the indexing positions.

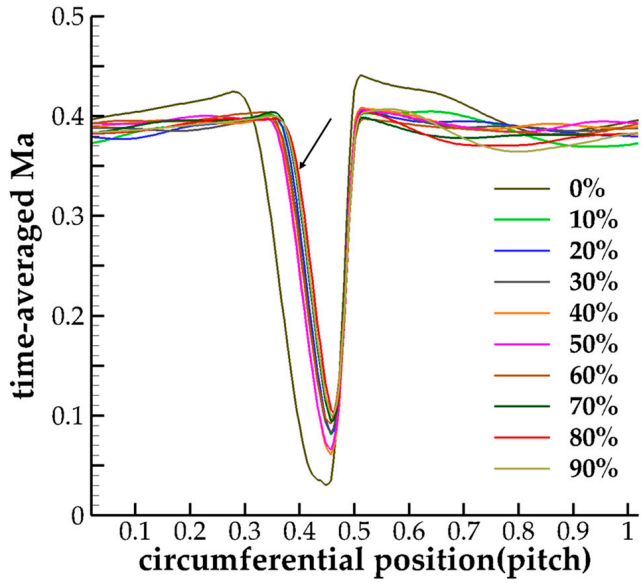


Figure 34. Time-averaged Ma after the TE of S1.

4.2.4. Modification Plan 4: Wake Angle

The wake angle is defined as the angle between the slip velocity and axial direction. Based on the baseline stage, the stagger angle is increased by 31 degrees, and the rotational speed of R1 is increased to 1.5× to ensure that the incoming Mach number and incidence of R1 are similar to those of Wake3_HL. Moreover, the blade number of S0 is reduced to two-thirds of the original value to ensure that the reduced frequency remains unchanged. The plan is called plan4_1. Similarly, in the comparison plan, the stagger angle is reduced by 13 degrees, and the rotational speed is reduced to 0.86×. The blade number of S1 is unchanged, so the reduced frequency of wake is reduced, and this plan is called plan4_2. Figure 35 shows the modification plan 4. During the calculation process, it is still necessary to set three wake strengths for comparative analysis.

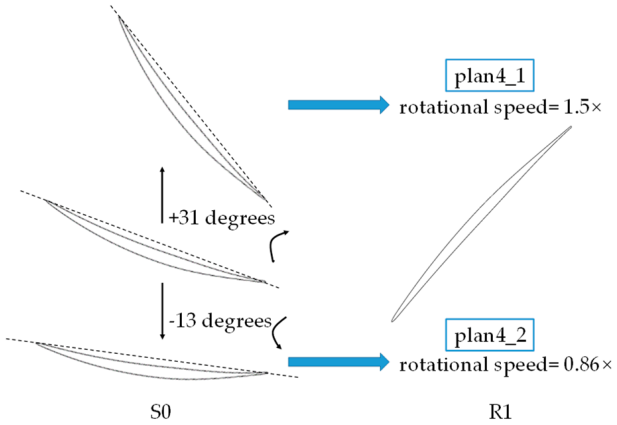


Figure 35. Modification plan 4.

Figure 36 demonstrates a specially selected case of SFAF with a relatively good effect. The effect of SFAF is inferior to Wake3_HL. The principal reason is depicted in Figure 20c, which reveals an insufficient pressure gradient in the direction of wake transport, so the local low-pressure region generated by the transport cannot induce a large velocity increment in SFAF. Meanwhile, even if SFAF has a velocity increment equivalent to Wake3_HL, according to the velocity triangle, the relationship of the decrease in absolute flow angle between plan 4_1 and Wake3_HL is uncertain due to the increase in rotational velocity.

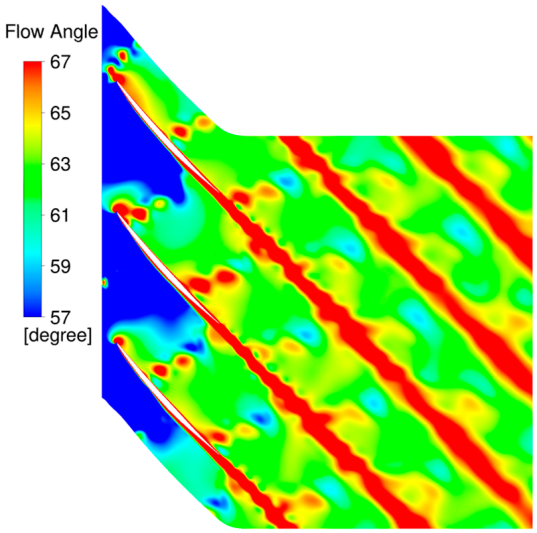


Figure 36. Absolute flow angle of modification plan 4_1.

Figure 37 illustrates the absolute flow angle of a specially selected case of plan 4_2, which presents similar results to Wake3_HL, indicating that SFAF near the TE is strong enough and larger than LFAF. Nevertheless, its size and strength rapidly increased, and under the mixing effect with SFAF, both SFAF size and strength decreased. The 80% axial chord in Figure 38 indicates that the local high-pressure region generated by the high-pressure fluid transport in the wake strengthens LFAF. Compared with Figure 20b, when the wake angle decreases, the pressure gradient in the transport direction is relatively large when the wake undergoes high-pressure transport at the rear end of the passage. This is a major disadvantage for generating an effective SFAF. The calculation of matching an S1 also confirms that the SFAF effect is not particularly significant.

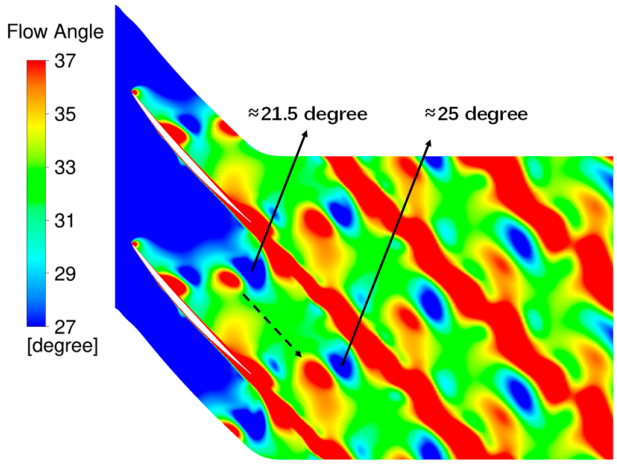


Figure 37. Absolute flow angle of modification plan 4_2.

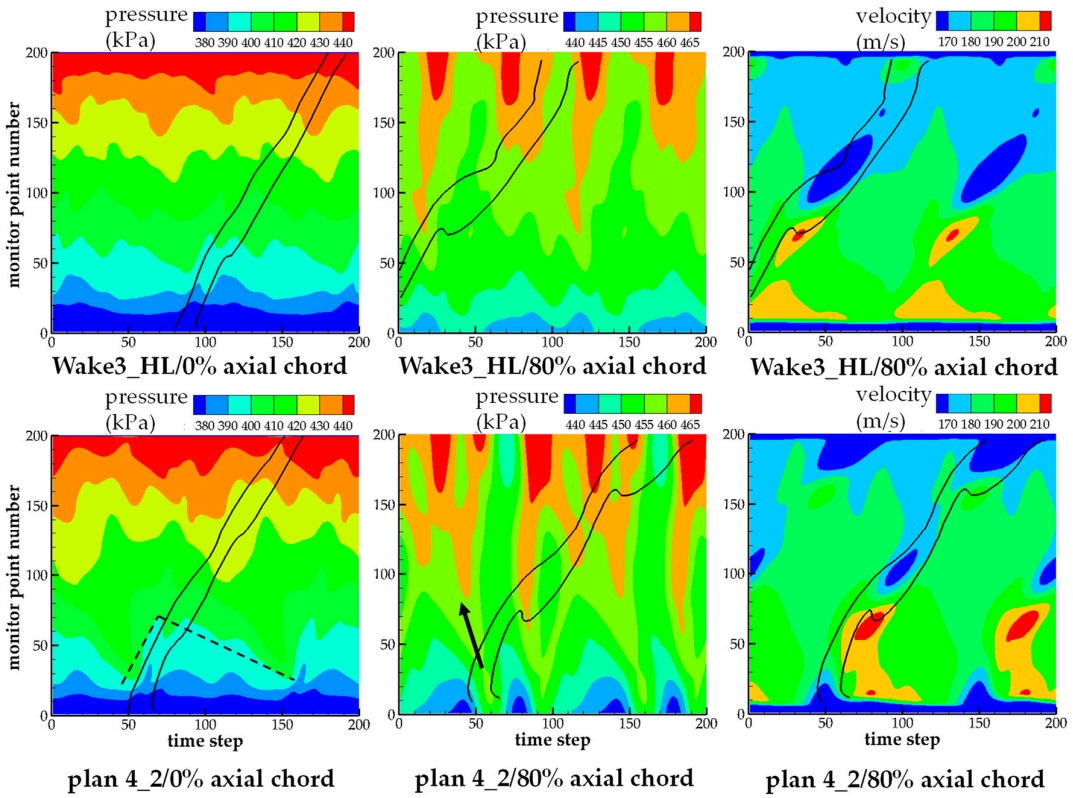


Figure 38. Time-varying pressure and velocity of Wake3_HL and plan 4_2.

The comparison of static pressure at 0% axial chord indicates that the distribution of static pressure near the suction surface over time is not as uniform as Wake3_HL, and the sweep of the wake leads to an increase in the proportion of the total R1 load, indicating that reducing the stagger angle of S0 can improve this effect. If the time-averaged load of the rotor is consistent, when the R1 load generated by the upstream wake increases, the load generated by the bulk flow naturally decreases, and the difference between the two causes a greater pressure drop on the suction surface with the wake impacting the LE, increasing the pressure difference between the low-pressure region generated by wake transport and the fluid in the adjacent region. Increasing the number of S0 blades based on plan 4_2 to amplify the wake-reduced frequency can also improve this effect. However, the result in Section 4.2.1 indicated the side effect of high reduced frequency, which was also validated in this study and confirmed inappropriate.

We modify the rotational speed of plan 4_2 to 1× to increase the load level appropriately, which is called plan 4_3. Figure 39 shows that although the size of SFAF is not as big as that of LFAF, the reduction in flow angle is significant. Figure 40 indicates a significant increase in the proportion of rotor load generated by the wake. The performance results of matching S1 indicate that the indexing position of 10% pitch obtains the maximum efficiency, and the configuration leads SFAF to impact the LE of S1, as shown in Figure 41. Thus, when the load of R1 is sufficient, the smaller the angle between the wake angle and the relative flow angle, the more obvious the effect of SFAF. From a design perspective, the two can be represented by a small difference in stagger angle.

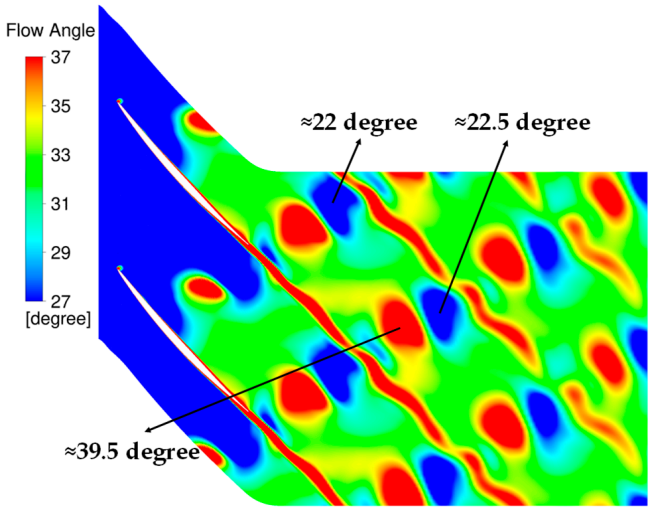


Figure 39. Absolute flow angle of modification plan 4_3.

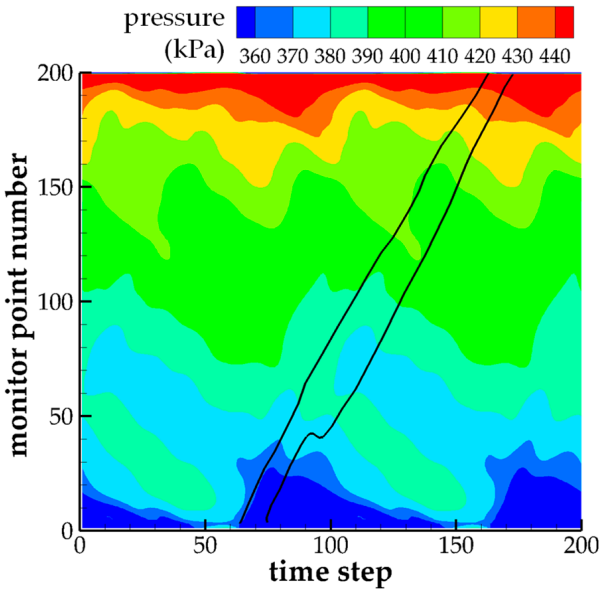


Figure 40. Time-varying pressure of modification plan 4_3 at 0% axial chord.

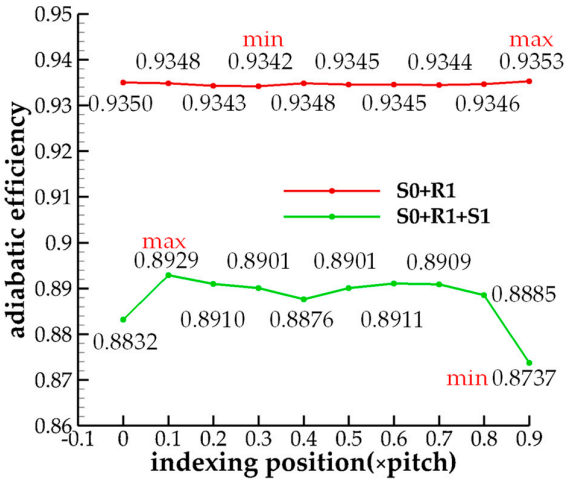


Figure 41. The performance of modification plan 4_3 with the indexing positions.

5. Conclusions and Perspectives

This paper performs two-dimensional RANS and URANS calculations in a series of subsonic compressor element stages to explore the mechanism of clocking effect and its influence on performance. Steady analysis and unsteady validation are used to explore trends in loss relationships, and detailed unsteady flow analysis reveals a new impact mechanism.

In subsonic compressors, if potential interaction and transition are not considered, the key factors affecting performance are the mixing loss and wake-induced separation loss of the wake in the rear stator blade. The relationship between the two determines which indexing configuration can achieve the highest efficiency.

For general situations, when S1 is at medium to low load conditions with low separation loss, and there is significant mixing loss in the S0 wake entering S1, CLLE is the optimal configuration. When S1 is at high load condition, and the separation loss is significant, the S0 wake will strengthen S1 separation, so CLMP is the optimal configuration. At the same time, pure S0 wake always increases the separation of S1 wake and lowers the static pressure rise of S1.

The negative jet effect of S0 wake in R1 can transport low-pressure fluid from the acceleration section of the suction surface to the high-pressure region, forming a local low-pressure region, resulting in local acceleration upstream of the low-pressure region and a decrease in absolute airflow angle. This fluid cluster is called SFAF.

The rim work of R1 determines the overall degree of pressure reduction on the suction surface, so when the rim work is too low, the SFAF effect is insignificant. However, increasing the camber angle or the blade tangential speed is ineffective. For the determined geometry and speed of R1, the high load condition without significant separation of R1 can make the SFAF effect more obvious, and in other words, the fore-loading condition can cause a greater pressure drop near the LE. Simultaneously, using a fore-loading blade profile is an effective means to improve the effectiveness of SFAF.

The strength of the S0 wake determines the transport strength, and too deep wake can transport the fluid in the high-pressure region to the relatively low-pressure position at the rear end of the passage, forming a local low-velocity region with a large absolute flow angle, thus weakening the effect of SFAF. At the same time, the reduced frequency of the S0 wake should not be too high. Otherwise, it will reduce the pressure gradient of the wake transport fluid and the bulk flow, weakening SFAF.

With the appropriate reduced frequency and rotor load, the matching relationship between the stagger angle of S0 and R1 determines the distribution relationship between the amount caused by the bulk flow and S0 wake in the R1 load. When the angle between the two blade chords in the axial direction is smaller, the proportion of R1 load caused by the S0 wake increases. That is, the pressure difference between the low-pressure region induced by the wake and the bulk flow is larger, and the acceleration of SFAF is stronger.

Furthermore, the circumferential non-uniformity of the S0 outlet flow changes the R1 pressure field, which can also affect SFAF.

In essence, both the wake and the circumferential non-uniform bulk flow can be considered as circumferential non-uniform inflow, and their impact on the spatiotemporal distribution characteristics of the pressure and velocity field in the blade passage needs to be explored as much as possible in the future work to clarify the effects of changes in parameters such as blade profile, blade load, wake reduced frequency, wake angle, and wake velocity deficit, and to determine the specific quantification range. The non-uniformity of pressure value over time at every position is very noteworthy, as well as its impact on the radial transport of three-dimensional flow in a stage environment.

Author Contributions: Conceptualization, H.N.; data curation, H.N.; formal analysis, H.N.; funding acquisition, J.C.; investigation, H.N.; methodology, H.N.; project administration, J.C.; resources, J.C.; software, H.N.; supervision, J.C.; validation, H.N.; visualization, H.N.; writing—original draft, H.N.; writing—review and editing, H.N. and H.X. All authors have read and agreed to the published version of the manuscript.

Funding: This research was funded by National Science and Technology Major Project, China (J2019-II-0005-0025).

Institutional Review Board Statement: Not applicable.

Informed Consent Statement: Not applicable.

Data Availability Statement: All the data produced in this study are contained in the manuscript text.

Conflicts of Interest: The authors declare no conflict of interest.

Abbreviations

Nomenclature

$\overline{\omega}$	time-averaged total pressure loss coefficient
C_p	pressure rise coefficient
$\overline{\eta}$	time-averaged isentropic efficiency
$\overline{p^*}$	time-averaged total pressure
$\overline{p}$	time-averaged pressure
$\overline{T^*}$	time-averaged total temperature
k	specific heat ratio
F_r	reduced frequency
u	tangential speed of rotor
t	pitch
w	relative velocity
c	chord length
β_{1k}	inlet blade angle
β_{2k}	outlet blade angle
$\Delta\beta_k$	camber angle
γ	stagger angle
d_{max}	maximum thickness
x_{max}	maximum thickness position

Subscripts

in	inlet
out	outlet

References

1. Walker, G.J.; Oliver, A.R. The Effect of Interaction Between Wakes from Blade Rows in an Axial Flow Compressor on the Noise Generated by Blade Interaction. *J. Eng. Power* **1972**, *94*, 241–248. [CrossRef]
2. Dorney, D.; Sharma, O. A Study of Turbine Performance Increases through Airfoil Clocking. In Proceedings of the 32nd Joint Propulsion Conference and Exhibit, Lake Buena Vista, FL, USA, 1 July 1996; American Institute of Aeronautics and Astronautics: Lake Buena Vista, FL, USA, 1996.

3. Reinmöller, U.; Stephan, B.; Schmidt, S.; Niehuis, R. Clocking Effects in a 1.5 Stage Axial Turbine—Steady and Unsteady Experimental Investigations Supported by Numerical Simulations. *J. Turbomach.* **2002**, *124*, 52–60. [CrossRef]
4. Jouini, D.B.M.; Little, D.; Bancalari, E.; Dunn, M.; Haldeman, C.; Johnson, P.D. Experimental Investigation of Airfoil Wake Clocking Impacts on Aerodynamic Performance in a Two Stage Turbine Test Rig. In Proceedings of the Volume 6: Turbo Expo 2003, Parts A and B; ASMEDC: Atlanta, GA, USA, 2003; pp. 351–358.
5. Smith, N.R.; Key, N.L. Vane Clocking Effects on Stator Loss for Different Compressor Loading Conditions. *J. Propuls. Power* **2015**, *31*, 519–526. [CrossRef]
6. Smith, N.R.; Key, N.L. Vane Clocking Effects on Stall Margin in a Multistage Compressor. *J. Propuls. Power* **2013**, *29*, 891–898. [CrossRef]
7. Key, N.L.; Lawless, P.B.; Fleeter, S. An Experimental Study of Vane Clocking Effects on Embedded Compressor Stage Performance. *J. Turbomach.* **2010**, *132*, 011018. [CrossRef]
8. Key, N.L.; Lawless, P.B.; Fleeter, S. An Investigation of the Flow Physics of Vane Clocking Using Unsteady Flow Measurements. In Proceedings of the Volume 6: Turbomachinery, Parts A, B, and C; ASMEDC: Berlin, Germany, 2008; pp. 2003–2014.
9. Smith, N.R.; Key, N.L. A Comprehensive Investigation of Blade Row Interaction Effects on Stator Loss Utilizing Vane Clocking. *J. Turbomach.* **2018**, *140*, 071004. [CrossRef]
10. Städing, J.; Wulff, D.; Kosyna, G.; Becker, B.; Gümmer, V. An Experimental Investigation of Stator Clocking Effects in a Two-Stage Low-Speed Axial Compressor. In *Proceedings of the Volume 7: Turbomachinery, Parts A, B, and C*; ASMEDC: Vancouver, BC, Canada, 2011; pp. 1563–1574.
11. Städing, J.; Friedrichs, J.; Waitz, T.; Dobriloff, C.; Becker, B.; Gümmer, V. The Potential of Rotor and Stator Clocking in a 2.5-Stage Low-Speed Axial Compressor. In *Proceedings of the Volume 8: Turbomachinery, Parts A, B, and C*; American Society of Mechanical Engineers: Copenhagen, Denmark, 2012; pp. 2453–2466.
12. Dorney, D.J.; Sharma, O.P.; Gundy-Burlet, K.L. Physics of Airfoil Clocking in a High-Speed Axial Compressor. In *Proceedings of the Volume 1: Turbomachinery*; American Society of Mechanical Engineers: Stockholm, Sweden, 1998; p. V001T01A024.
13. Gundy-Burlet, K.L.; Dorney, D.J. Physics of Airfoil Clocking in Axial Compressors. In *Proceedings of the Volume 4: Manufacturing Materials and Metallurgy; Ceramics; Structures and Dynamics; Controls, Diagnostics and Instrumentation; Education; IGTI Scholar Award*; American Society of Mechanical Engineers: Orlando, FL, USA, 1997; p. V004T14A058.
14. Gundy-Burlet, K.; Dorney, D.; Gundy-Burlet, K.; Dorney, D. Investigation of Airfoil Clocking and Inter-Blade-Row Gaps in Axial Compressors. In Proceedings of the 33rd Joint Propulsion Conference and Exhibit, Seattle, WA, USA, 6 July 1997; American Institute of Aeronautics and Astronautics: Seattle, WA, USA, 1997.
15. Huang, H.; Yang, H.; Feng, G.; Wang, Z. Fully Clocking Effect in a Two-Stage Compressor. In *Proceedings of the Volume 6: Turbo Expo 2003, Parts A and B*; ASMEDC: Atlanta, GA, USA, 2003; pp. 1051–1061.
16. Huang, H.; Yang, H.; Feng, G.; Wang, Z. Clocking Effect in a Two-Stage Compressor with Different Inter-Blade-Row Gaps. *J. Therm. Sci.* **2004**, *13*, 8–15. [CrossRef]
17. Key, N.L. Compressor Vane Clocking Effects on Embedded Rotor Performance. *J. Propuls. Power* **2014**, *30*, 246–248. [CrossRef]
18. Mileshin, V.I.; Savin, N.M.; Kozhemyako, P.G.; Druzhinin, Y.M. Numerical and Experimental Analysis of Radial Clearance Influence on Rotor and Stator Clocking Effect by Example of Model High Loaded Two Stage Compressor. In *Proceedings of the Volume 2A: Turbomachinery*; American Society of Mechanical Engineers: Düsseldorf, Germany, 2014; p. V02AT37A037.
19. Mileshin, V.; Druzhinin, I.; Savin, N.; Kozhemyako, P. Numerical and Experimental Studies of Reynolds Number and Stator Clocking Effect on Performance of a High-Loaded Two-Stage Compressor with 3.7 Total Pressure Ratio. In *Proceedings of the Volume 2D: Turbomachinery*; American Society of Mechanical Engineers: Seoul, Republic of Korea, 2016; p. V02DT44A011.
20. Layachi, M.Y.; Bölcs, A. Effect of the Axial Spacing Between Rotor and Stator with Regard to the Indexing in an Axial Compressor. In *Proceedings of the Volume 1: Aircraft Engine; Marine; Turbomachinery; Microturbines and Small Turbomachinery*; American Society of Mechanical Engineers: New Orleans, LA, USA, 2001; p. V001T03A089.
21. He, L.; Chen, T.; Wells, R.G.; Li, Y.S.; Ning, W. Analysis of Rotor-Rotor and Stator-Stator Interferences in Multi-Stage Turbomachines. *J. Turbomach.* **2002**, *124*, 564–571. [CrossRef]
22. Fruth, F.; Vogt, D.M.; Bladh, R.; Fransson, T.H. Unsteady Forcing vs. Efficiency: The Effect of Clocking on a Transonic Industrial Compressor. In *Proceedings of the Volume 1A, Symposia: Advances in Fluids Engineering Education; Advances in Numerical Modeling for Turbomachinery Flow Optimization; Applications in CFD; Bio-Inspired Fluid Mechanics; CFD Verification and Validation; Development and Applications of Immersed Boundary Methods; DNS, LES, and Hybrid RANS/LES Methods*; American Society of Mechanical Engineers: Incline Village, NV, USA, 2013; p. V01AT02A010.
23. Jia, H.; Vogeler, K. Effect of Clocking on the Unsteady Rotor Blade Loading in a 1.5-Stage Low-Speed Axial Compressor. In *Proceedings of the Volume 6: Turbo Expo 2007, Parts A and B*; ASMEDC: Montreal, QC, Canada, 2007; pp. 1599–1609.
24. Hsu, S.T.; Wo, A.M. Reduction of Unsteady Blade Loading by Beneficial Use of Vortical and Potential Disturbances in an Axial Compressor with Rotor Clocking. *J. Turbomach.* **1998**, *120*, 705–713. [CrossRef]
25. Mailach, R.; Vogeler, K. Rotor-Stator Interactions in a Four-Stage Low-Speed Axial Compressor—Part I: Unsteady Profile Pressures and the Effect of Clocking. *J. Turbomach.* **2004**, *126*, 507–518. [CrossRef]
26. Jia, H.; Xi, G.; Müller, L.; Mailach, R.; Vogeler, K. Unsteady Blade Loading with Clocking in Multistage Axial Compressors, Part 1. *J. Propuls. Power* **2010**, *26*, 25–35. [CrossRef]

27. Müller, L.; Mailach, R.; Vogeler, K.; Jia, H.; Xi, G. Unsteady Blade Loading with Clocking in Multistage Axial Compressors, Part 2. *J. Propuls. Power* **2010**, *26*, 36–45. [CrossRef]
28. Barankiewicz, W.S.; Hathaway, M.D. Effects of Stator Indexing on Performance in a Low Speed Multistage Axial Compressor. In *Proceedings of the Volume 1: Aircraft Engine; Marine; Turbomachinery; Microturbines and Small Turbomachinery*; American Society of Mechanical Engineers: Orlando, FL, USA, 1997; p. V001T03A098.
29. Reid, L.; Moore, R. *Performance of Single-Stage Axial-Flow Transonic Compressor with Rotor and Stator Aspect Ratios of 1.19 and 1.26, Respectively, and with Design Pressure Ratio of 1.82*; Technical Publication NASA-TP-1338; NASA: Washington, DC, USA, 1978.
30. Wei, Z.; Ni, M.; Gan, X.; Chen, W.; Chen, P. Generation of Unsteady Incoming Wakes for Wake/Blade Interaction. *Aerosp. Sci. Technol.* **2020**, *106*, 106127. [CrossRef]
31. Estevadeordal, J.; Gorrell, S.E.; Copenhaver, W.W. PIV Study of Wake-Rotor Interactions in a Transonic Compressor at Various Operating Conditions. *J. Propuls. Power* **2007**, *23*, 235–242. [CrossRef]
32. Niu, H.; Chen, J.; Xiang, H. Effect of Rotor-Stator Spacing on Compressor Performance at Variable Operating Conditions. *Appl. Sci.* **2022**, *12*, 6932. [CrossRef]

Disclaimer/Publisher's Note: The statements, opinions and data contained in all publications are solely those of the individual author(s) and contributor(s) and not of MDPI and/or the editor(s). MDPI and/or the editor(s) disclaim responsibility for any injury to people or property resulting from any ideas, methods, instructions or products referred to in the content.